MICROBIOLOGY

A *Plasmodium* membrane receptor platform integrates cues for egress and invasion in blood forms and activation of transmission stages

Ronja Marie Kuehnel[1]†, Emma Ganga[1]†, Aurélia C. Balestra[1]†‡, Catherine Suarez[1], Matthias Wyss[2,3], Natacha Klages[1], Lorenzo Brusini[1], Bohumil Maco[1], Nicolas Brancucci[2,3], Till S. Voss[2,3], Dominique Soldati[1], Mathieu Brochet[1]*

Critical events in the life cycle of malaria-causing parasites depend on cyclic guanosine monophosphate homeostasis by guanylyl cyclases (GCs) and phosphodiesterases, including merozoite egress or invasion of erythrocytes and gametocyte activation. These processes rely on a single GCα, but in the absence of known signaling receptors, how this pathway integrates distinct triggers is unknown. We show that temperature-dependent epistatic interactions between phosphodiesterases counterbalance GCα basal activity preventing gametocyte activation before mosquito blood feed. GCα interacts with two multipass membrane cofactors in schizonts and gametocytes: UGO (unique GC organizer) and SLF (signaling linking factor). While SLF regulates GCα basal activity, UGO is essential for GCα up-regulation in response to natural signals inducing merozoite egress and gametocyte activation. This work identifies a GC membrane receptor platform that senses signals triggering processes specific to an intracellular parasitic lifestyle, including host cell egress and invasion to ensure intraerythrocytic amplification and transmission to mosquitoes.

INTRODUCTION

Malaria is caused by vector-borne unicellular parasites of the genus *Plasmodium* that cycle between mosquito and vertebrate hosts. Malaria pathology is linked to the proliferation of asexual blood stages with waves of fever arising from the synchronized egress of merozoites from erythrocytes. Transmission from human to the mosquito is mediated by an obligatory sexual life cycle phase. Differentiation from asexually replicating stages into nondividing male and female gametocytes takes place inside red blood cells (RBCs). Following a period of maturation, the sexual precursors are ready to initiate transmission when ingested by a mosquito. Both processes are tightly regulated as premature or late egress that lead to noninvasive merozoites (*1*), and successful gametogenesis has to rapidly happen only upon ingestion by a mosquito.

Distinct signals have been associated to merozoite egress and gametocyte activation. Gametocytes differentiate into gametes via at least three environmental factors upon ingestion by a mosquito. A drop in temperature is experienced by the parasite as it leaves the vertebrate blood stream and is essential for gamete formation in vitro (*2*). However, efficient activation of gametogenesis in vivo requires xanthurenic acid (XA) (*3*, *4*), a product of the oxidative metabolism of tryptophan that is present in the mosquito midgut (*5*), with increasing concentration upon ingestion of a blood meal (*6*). It was also shown that a small rise of 0.2 to 0.3 pH units in the blood meal happens during the first half hour after feeding, which potentiates the effect of XA (*7*). Signals triggering merozoite egress are less well defined and may involve a wide range of cues, possibly including parasite or host circadian rhythms (*8*, *9*) that dictate intracellular pathways mediated by protein phosphatase 1 in response to exposition to cues such as phosphatidylcholine (PC) (*10*).

Signal perception from the environment and integration to the interior of a cell is essential for all forms of life. Different cells use distinct receptors to mediate transmembrane signaling such as sensor histidine kinases in bacteria (*11*), G protein–coupled receptors (*12*) and receptor kinases (*13*) in animals or yeasts, and specific receptor kinases in plants (*14*). *Plasmodium*, as a member of the Apicomplexa phylum, is phylogenetically distant from these organisms (*15*, *16*), and these sensors are not found in this parasite. As a consequence, it remains a mystery how signals triggering egress or gametogenesis are sensed by *Plasmodium*.

Merozoite egress and gametocyte activation both require the mobilization of intracellular calcium following the activation of the cyclic guanosine monophosphate (cGMP)–dependent protein kinase (*17*) by elevation of cGMP levels (*18*). This indicates that regulation of cGMP levels by guanylyl cyclases (GCs) and phosphodiesterases (PDEs) is key to the integration of external signals to initiate merozoite egress or activate gametogenesis. In well-studied eukaryotes such as metazoans, yeasts, and plants, GCs exist in two main forms. The receptor form displays a single-membrane-spanning domain that binds directly to extracellular ligands such as peptide hormones, whereas the soluble cytosolic forms are activated by membrane-soluble nitric oxide (*19*). *Plasmodium* parasites encode two transmembrane cGMP-producing GCs (GCα and GCβ). Both GCs are atypical compared with other eukaryotic GC receptors in the sense that they are composed of two GC catalytic domains fused to a P4–adenosine triphosphatase (ATPase) domain that may be responsible for phospholipid binding or flipping across membrane leaflets (*20*, *21*). Disruption of *GCβ* in multiple *Plasmodium* species did not impair merozoite egress or gametogenesis

[1]Department of Microbiology and Molecular Medicine, Faculty of Medicine, University of Geneva, 1 Rue Michel Servet, 12111 Geneva, Switzerland. [2]Department of Medical Parasitology and Infection Biology, Swiss Tropical and Public Health Institute, 4123 Allschwil, Switzerland. [3]University of Basel, 4001 Basel, Switzerland.
*Corresponding author. Email: mathieu.brochet@unige.ch
†These authors contributed equally to this work.
‡Present address: Department of Pathobiology, School of Veterinary Medicine, University of Pennsylvania, Philadelphia, PA, USA.

(*22*–*24*). Instead, GCα was shown to be essential for the elevation of cGMP levels required for merozoite egress in *Plasmodium falciparum* (*25*) and gametocyte activation in *Plasmodium yoelii* (*26*). As both processes are induced by different signals but commonly rely on cGMP production by GCα, this raises the question as to how distinct cues regulate the same pathway. This could possibly be explained by stage-specific cofactors differentially regulating GCα activity in response to stage-specific cues. For example, the activity of GCα in gametocytes was shown to require a GCα-interacting protein named gametogenesis essential protein 1 (GEP1), while GEP1 was not required for proliferation of asexual blood stages (*26*). However, as *gep1* deletion abolished GCα basal activity in gametocytes, its possible role in signal perception could not be assessed. It thus remains unknown how extracellular signals modulate the activity of *Plasmodium* GCs.

Stage-specific regulation of cGMP homoeostasis may also rely on differential expression or activity of the four cGMP-degrading PDEs (*27*, *28*). Deletion of *PDE*α, *PDE*γ, or *PDE*δ did not lead to obvious phenotypes in the proliferation of asexual blood stages in both *P. falciparum* and *Plasmodium berghei* (*29*). In contrast, conditional depletion of PDEβ causes a profound reduction in invasion of erythrocytes and rapid death of those merozoites that invade, but no obvious egress phenotype was observed (*28*), suggesting that deletion or depletion of a single PDE does not affect natural merozoite egress in in vitro cultures. However, treatment with zaprinast, a PDE inhibitor of human PDE5, PDE6, PDE9, and PDE11, raises cellular cGMP levels and triggers egress, suggesting that cGMP degradation is at least important to prevent premature merozoite egress (*1*). Similarly, zaprinast stimulates gametogenesis (*30*), and deletion of *PDE*δ in *P. falciparum* led to a twofold increase in cellular cGMP levels in late-stage gametocytes and defective gametogenesis (*22*), suggesting that cGMP degradation prevents premature activation and associated deleterious effects on gamete formation. Deletion of *PDE*δ in *P. berghei* had no effect on gamete formation, raising the possibility that another PDE might compensate for its absence in this species. Deletion of *PDE*γ had no effect on gametogenesis, and the requirement for PDEβ or PDEα during gametogenesis has not yet been investigated in detail.

Using gametocytes as a signaling paradigm for cGMP homeostasis, we first revisit the role of temperature by showing that temperature itself does not act as a signal but as a factor necessary for the developmental changes following activation by XA and pH. We then show that epistatic interactions between two cGMP-degrading PDEs efficiently degrade basal levels of cGMP, thus preventing premature activation before a mosquito feed. To identify proteins involved in sensing mosquito signals, we then turn our attention to the regulation of cGMP production by GCα and identify two important membrane cofactors that are important for either basal activity or induced activity in response to environmental signals. We further show that activity of this GC platform is also induced by different signals to trigger merozoite egress. Last, we provide evidence that the properties of the membranes hosting this platform may also contribute to modulate its activity in response to environmental signals.

RESULTS

XA or a rise in pH triggers calcium mobilization in *P. berghei* gametocytes independently of temperature

XA is known to facilitate initiation of gametogenesis both in vitro and in vivo at a permissive temperature (*3*, *31*, *32*) via the mobilization of intracellular calcium following elevation of cGMP levels (*33*–*35*). It is however unknown whether XA is also active at a nonpermissive temperature. To compare the activity of XA at 37° and 20°C, *P. berghei* gametocytes were collected at 37°C and maintained in a suspended animation (SA) medium that prevents activation at both 37° and 20°C because of a pH of 7.2 and the absence of XA. One-half of the gametocytes was kept at 37°C, while the other half was cooled down to 20°C. Following gametocyte purification, we then monitored intracellular calcium upon activation with 100 μM XA or an increase to pH 7.8 at both temperatures using the Fluo-4 acetoxymethyl ester (AM) calcium indicator (Fig. 1, A to C). A similar calcium response to XA or a rise in pH was observed at 20° and 37°C with no notable change in three of the four quantified parameters: the area under the curve (AUC), the maximum response 30 s postactivation (Y_{Max}), or the intensity 5 min postactivation (Y_{300}). However, the time to reach the maximum intensity (T_{Max}) was almost halved for both stimuli at 37°C (fig. S1, A and B), suggestive of a higher GC activity and/or a lower PDE activity at 37°C (Fig. 1D).

Despite the observed calcium mobilization, gametocytes stimulated at 37°C did not further develop into gametes as opposed to those maintained at 20°C (Fig. 1E), as previously described (*2*). This defect is linked to an early block of DNA replication upon activation by XA and a rise in pH to 7.8 at 37°C (Fig. 1F). These results suggest that a decrease in temperature is important for pathways following calcium mobilization but does not act as a signal to activate the cGMP/calcium signaling module. To confirm this hypothesis, we injected 20 μl of 37°C SA (no XA; pH 7.2) containing gametocytes expressing the GFP-aequorin calcium reporter (*35*) into 20 μl of SA at 4°C (no XA; pH 7.2), leading to a final temperature of 20.5°C. No calcium mobilization could be observed up to 60 s posttreatment (Fig. 1G). Exposing gametocytes to 100 μM XA or to a pH of 7.8 led to calcium mobilization, indicating that gametocytes are responsive under these experimental conditions. Together, this indicates that XA and elevated pH trigger gametocyte activation at permissive and nonpermissive temperatures. However, a decrease in temperature is not sufficient for gametocyte activation in the absence of XA or a rise in pH but is essential for the formation of gametes following activation.

PDEα and PDEδ show temperature-dependent activities in *P. berghei* gametocytes

Calcium mobilization requires the rapid elevation of cGMP levels (*18*). We thus set out to investigate the relative roles of PDEs in the timely activation of gametocytes. We first individually knocked out each of the three genes coding for PDEα, PDEγ, and PDEδ, which were previously shown to be dispensable for asexual proliferation in erythrocytes (fig. S2, A and B) (*22*, *23*, *29*, *36*). Knockout (KO) clonal lines were obtained, and no defects in exflagellation were observed upon stimulation by XA and pH elevation (Fig. 2A), suggesting that these PDEs are not directly regulated by XA or pH. However, the PDEδ-KO line showed a significantly different calcium response to XA and pH at 20°C with a slower decay and a larger AUC (Fig. 2, B to D, and fig. S2C), indicating that PDEδ

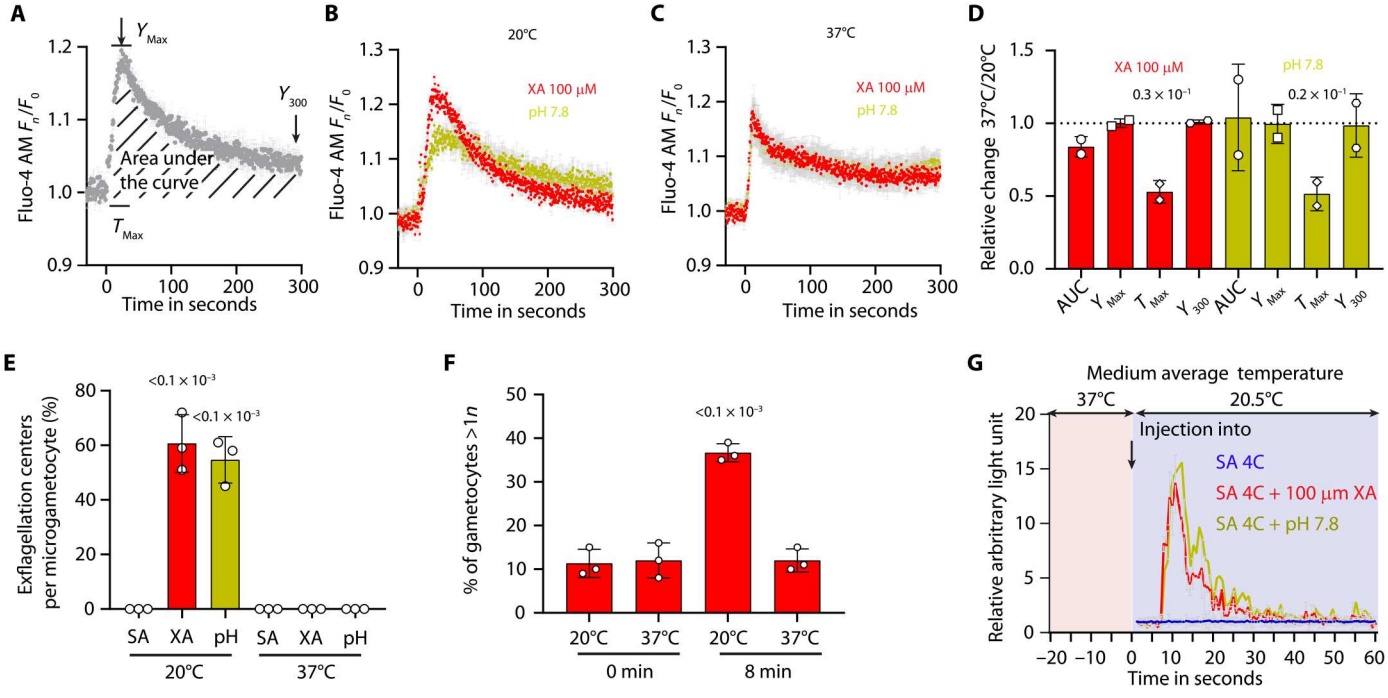

Fig. 1. XA and a rise in extracellular pH activate calcium mobilization at 37° and 20°C in *P. berghei* gametocytes, while a drop in temperature is essential later for DNA replication. (**A**) Fluorescence response kinetics of gametocytes loaded with Fluo-4 AM upon stimulation with 100 µM XA and illustration of the different parameters used for the quantification of calcium mobilization (SD; *n* = 3 technical replicates). (**B** and **C**) Fluorescence response upon stimulation with 100 µM XA or a rise from pH 7.2 to 7.8 at 20°C (B) and 37°C (C) (SD; *n* = 3 technical replicates). (**D**) Relative changes in calcium response at 37°C compared to 20°C upon stimulation with 100 µM XA or rise from pH 7.2 to 7.8 indicate that the time to reach the maximum calcium response is faster at 37°C (SD; *n* = 2 biological replicates, unpaired two-tailed *t* test). (**E**) Gametocyte activation with 100 µM XA or rise from pH 7.2 to 7.8 does not allow microgamete formation at 37°C, whereas the same stimuli at 20°C leads to formation of microgametes [SD; *n* = 3 technical replicates, one-way analysis of variance (ANOVA)]. (**F**) Proportion of haploid or multiploid gametocytes in nonactivated and 8-min activated gametocytes at 20° or 37°C shows that DNA replication is blocked at 37°C (SD; *n* = 3 biological replicates, one-way ANOVA). (**G**) Dilution of gametocytes maintained in SA medium (SA) at 37°C into a cold SA medium leading to a rapid decrease to 20.5°C is not sufficient to induce a rapid calcium response. Dilution into the same SA containing either 100 µM XA or at a pH of 7.8 leads to normal calcium mobilization.

is involved in lowering calcium levels following initial mobilization. All three lines showed a similar response to the calcium ionophore A23187, indicating that calcium available for mobilization was not affected (fig. S2D).

As PDEβ was previously shown to be essential for the growth of asexual blood stages (*28*), we tagged the endogenous *PDE*β with hemagglutinin (HA) epitope tag and an auxin-inducible degron (AID) (fig. S2E) to degrade the fusion protein in the presence of auxin in a strain expressing the Tir1 protein (*37*). Western blot analysis indicated depletion of PDEβ-AID/HA upon auxin [or indole acetic acid (IAA)] treatment (fig. S2F), and yet, PDEβ-depleted gametocytes exflagellated upon stimulation by XA and elevated pH (fig. S2G), suggesting that PDEβ is not important to respond to XA or a rise in extracellular pH at a permissive temperature. It is however possible that lower levels of PDEβ-AID/HA may be sufficient to achieve its function in gametocytes.

5-Benzyl-3-isopropyl-1H-pyrazolo[4,3-d]pyrimidin-7(6H)-one (BIPPO) and zaprinast, two PDE inhibitors, triggered calcium mobilization at 20° and 37°C (Fig. 2, E and F), suggesting that at least one PDE is active and counteracts basal GC activity to prevent gametocyte activation in absence of XA or pH stimulation at both permissive and nonpermissive temperatures. We thus took advantage of the PDE-KO lines to infer which PDEs are targeted by these molecules (Fig. 2, G to L, and fig. S2, H and I). PDEδ-KO was fourfold less susceptible to 5 µM BIPPO at both 20° and 37°C. This indicates that PDEδ is the main target of BIPPO in gametocytes and is active at both 20° and 37°C. PDEα-KO gametocytes were less susceptible to zaprinast but only at 37°C, indicating that this inhibitor also targets PDEα, as previously described (*36*, *38*), and that this enzyme is more active at 37°C than at 20°C.

Epistatic interactions between PDEα and PDEδ prevent premature activation of *P. berghei* gametocytes

As both PDEα and PDEδ were found to be active at 37°C, we wondered whether simultaneous deletion of both enzymes would lead to premature and abortive activation of gametocytes. A PDEα/δ-KO clonal line (fig. S2A) did not show any obvious growth defect of asexual blood stages or growth defect in the formation of male and female gametocytes. However, activation of PDEα/δ-KO gametocytes with XA at 20°C did not lead to the formation of active exflagellation centers (Fig. 2M), and male gametogenesis was found to be blocked at an early stage as no DNA replication could be observed upon stimulation with XA and a rise in pH (fig. S2J). At 37°C, reduced calcium responses to zaprinast and BIPPO were further exacerbated in the PDEα/δ-KO line compared with parental PDEα-KO or PDEδ-KO gametocytes (Fig. 2, N and O, and fig. S2K). Parasites still responded to XA and elevated pH but with reduced and slower calcium mobilization. A similar but less marked

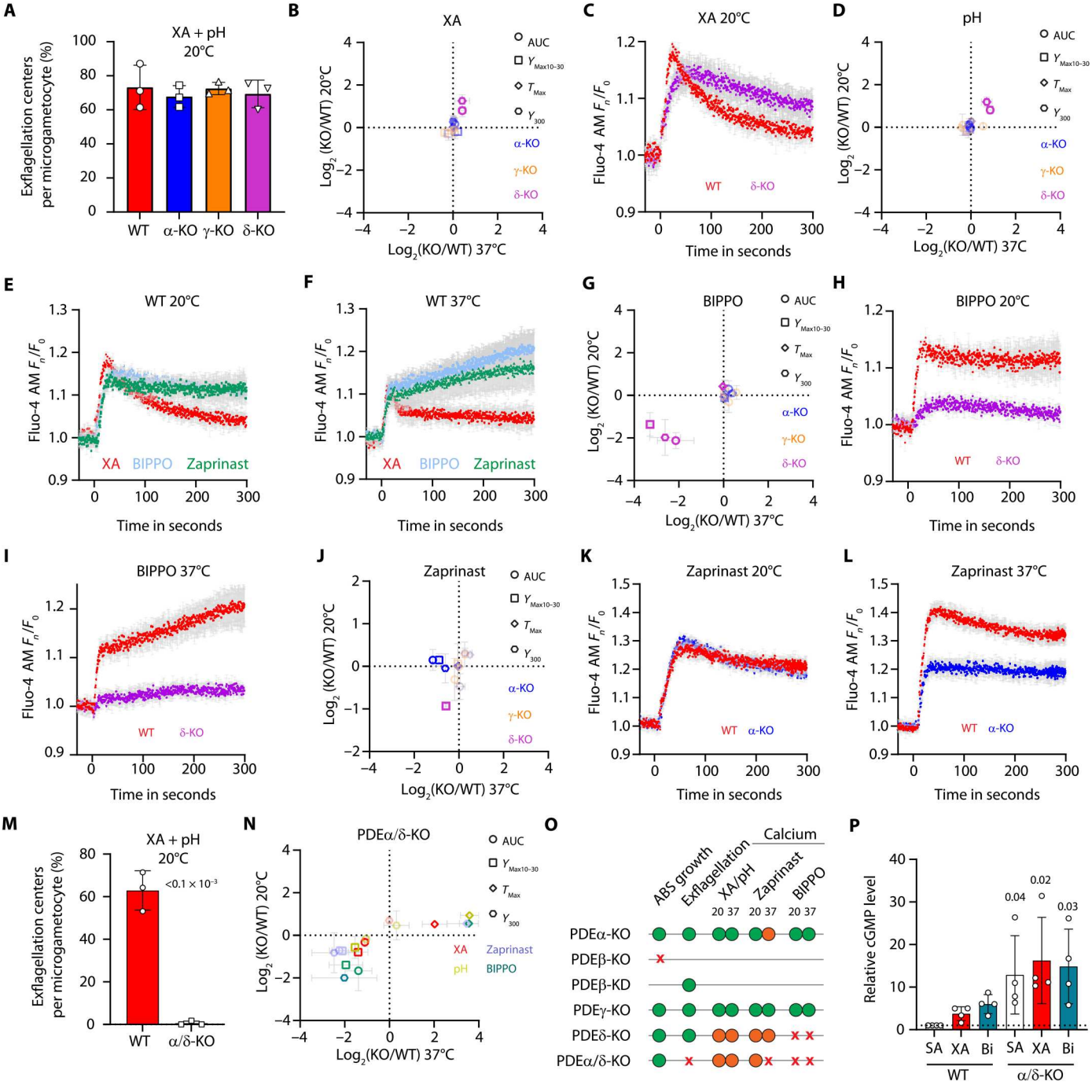

Fig. 2. PDEα and PDEδ are active at 37°C in gametocytes and epistatic interactions between both enzymes that prevent premature and abortive activation. (**A**) KOs of nonessential PDEs show normal exflagellation rates (SD; $n = 3$ biological replicates). (**B**) Comparison of the Ca^{2+} response of each PDE-KO to the wild type (WT). A shift toward the left reflects a decrease at 37°C in the KO compared to the WT. A shift below the horizontal line reflects a decrease at 20°C in the KO compared to the WT. The parameters used correspond to the parameters described in Fig. 1A (SD; $n = 3$ or $n = 2$ biological replicates at 20° and 37°C, respectively). (**C**) Fluorescence kinetics of WT and PDEδ-KO gametocytes upon stimulation with 100 μM XA. (**D**) A rise to pH 7.8 leads to similar response profiles observed with XA for each PDE-KO line. (**E** and **F**) Fluorescence kinetics of WT gametocytes upon stimulation at 20°C (E) or 37°C (F) (SD; $n = 3$ biological replicates). (**G**) Upon stimulation with 5 μM 5-benzyl-3-isopropyl-1H-pyrazolo[4,3-d]pyrimidin-7(6H)-one (BIPPO), a strong decrease of PDEδ-KO response is observed. (**H** and **I**) Fluorescence kinetics of WT and PDEδ-KO gametocytes upon stimulation with 5 μM BIPPO at 20°C (H) and 37°C (I) (SD; $n = 3$ technical replicates). (**J**) Upon stimulation with 500 μM zaprinast, a decrease of PDEα-KO response is observed at 37°C. (**K** and **L**) Fluorescence kinetics of WT and PDEα-KO gametocytes upon stimulation with 500 μM zaprinast at 20°C (K) or 37°C (L). (**M**) The simultaneous deletions of *PDEα* and *PDEδ* prevent microgametogenesis (SD; $n = 3$ biological replicates, unpaired two-tailed t test). (**N**) Comparison of the calcium response of PDEα/δ-KO gametocytes with WT at 37° and 20°C. (**O**) Summary of assessed PDE phenotypes. ABS, asexual blood stages; red crosses, affected; orange circles, mildly affected; green circles, not affected. (**P**) Relative basal and induced cGMP levels in WT and PDEα/δ-KO gametocytes (SD; $n = 2$ biological replicates with technical duplicates each, one-way ANOVA).

pattern of altered calcium responses was also observed at 20°C. This altered calcium mobilization was linked to ~12-fold higher cGMP levels in nonactivated PDEα/δ-KO gametocytes compared to the wild-type (WT) control line (Fig. 2P).

Together, these results demonstrate that neither PDEα nor PDEδ directly contribute to the elevation of cGMP levels in response to XA or pH. Instead, both enzymes are active at 37°C to prevent premature activation of gametocytes in the vertebrate host. Simultaneous deletion of *PDE*α and *PDE*δ likely leads to prolonged premature and abortive activation of gametogenesis due to sustained elevated cGMP levels at a nonpermissive temperature that leads to an early block between calcium mobilization and DNA replication in microgametocytes. This emphasizes an important and unexpected role of temperature in the efficient progression of DNA replication in microgametocytes.

GCα is required for calcium mobilization in response to XA or pH in *P. berghei* gametocytes

As synthesis of cGMP seems to be a limiting factor in the activation of gametocytes in response to XA or a rise in pH, we turned our attention to the two cGMP-producing GCs. GCβ was previously shown to be redundant for gamete formation (*22*, *23*). Analysis of a *GC*β-disrupted mutant (*23*) showed no calcium defect in response to XA, or PDE inhibitors in gametocytes both at 20° and 37°C (fig. S3A). Consistent with this observation, knocking down *GC*α in developing gametocytes previously revealed the crucial role of this GC in mediating XA response in *P. yoelii* (*26*). To study the role of GCα in *P. berghei* gametocytes, an AID/HA tag was added to the GCα C terminus (fig. S3B), which imposed a fitness cost, with low exflagellation rates even in the absence of auxin. However, a 1-hour treatment with auxin of gametocytes before activation led to a further significant reduction in exflagellation and calcium mobilization upon XA, pH, or BIPPO treatments (Fig. 3, A to D, and fig. S3C). Calcium response to the calcium ionophore A23187 was however normal, suggesting that the parasite calcium stores are not affected upon GCα-AID/HA depletion (Fig. 3D and fig. S3C). Together, these results confirm that, in gametocytes, GCα is the main GC responsible for basal or induced cGMP synthesis in response to XA or a rise in extracellular pH.

Coimmunoprecipitations identify a GCα membrane signaling platform in *P. berghei* gametocytes

The basal activity of GCα in *P. yoelii* gametocytes was recently shown to require a GCα-interacting protein named GEP1 (*26*). To look for other GCα partners, we used affinity purification of 3xHA-tagged GCα (fig. S3B) from nonactivated gametocytes under cross-linking conditions to identify interacting proteins (Fig. 3E and table S1). This identified GEP1 and also cell division control 50 (CDC50B) that were recently shown to interact with GCα in *P. falciparum* schizonts (*39*). CDC50 proteins usually act as chaperones to facilitate activity and/or trafficking of flippases to their final destination (*40*), suggesting that CDC50B may contribute to the regulation, folding, or trafficking of the predicted flippase domain of GCα. We also detected four peptides mapping on the unique GC organizer (UGO; PBANKA_1201400), a multipass membrane protein we previously identified by immunoprecipitating the single GC in *Toxoplasma gondii* and further showed to be essential for the unique GC activity and localization (*41*). To confirm the interaction between UGO and GCα in *P. berghei* gametocytes, UGO was tagged with 3xHA (fig. S3D). Affinity purification of UGO-3xHA recovered GCα as expected, but neither GEP1 nor CDC50B. In both GCα-HA and UGO-HA immunoprecipitates, we additionally detected PBANKA_0306700, the predicted ortholog of the signaling linking factor (SLF), another multipass membrane protein that we also previously found enriched in GC immunoprecipitates from *T. gondii* tachyzoites (*41*) and that was shown to be important for GC activity in *T. gondii* (*42*, *43*). We additionally detected at least two peptides mapping on five other proteins that likely represent nonspecific interactions (Fig. 3E and table S1). Together, this suggests that GCα is part of a conserved membrane signaling platform in *P. berghei* gametocytes and that the identified partners may play a role in regulating the activity of GCα.

SLF is a GCα-interacting protein important for its basal cGMP synthesis in *P. berghei* gametocytes

To investigate the role of CDC50B in gametocytes, a CDC50B-KO clonal line was generated (fig. S3E), and no obvious defects in exflagellation (fig. S3F) was observed, suggesting that CDC50B is dispensable for GCα activity. No SLF-KO line could be generated, suggesting an essential role in asexual blood stages. We therefore tagged the endogenous *slf* with an AID/HA epitope tag (fig. S3G) to degrade the fusion protein in the presence of auxin in a strain expressing the Tir1 protein (*37*). Following a 1-hour auxin treatment of gametocytes, depletion of SLF-AID/HA was observed by Western blot (Fig. 3F), associated with a twofold diminution of the exflagellation rate in response to XA and a rise in pH (Fig. 3G). Consistent with this observation, a twofold reduction in calcium mobilization was observed in response to XA, elevated pH, or BIPPO (Fig. 3H and fig. S3H), as well as lower induced cGMP levels 20 s following stimulation by XA or BIPPO (Fig. 3I). The limited signal above the detection level of SLF-AID/HA does not exclude residual presence of the protein. Nevertheless, these results showing reduced response to both natural signals and PDE inhibition point to a role of SLF in maintaining GCα basal activity. SLF-AID/HA was associated with a significant decrease in calcium response to A23187 that was not observed for GCα, suggesting an additional role of SLF in basal calcium homeostasis.

UGO is a GCα-interacting protein essential for its up-regulation upon stimulation by XA or pH in *P. berghei* gametocytes

No UGO-KO line could be generated, and we therefore fused UGO to an AID/HA tag at the endogenous locus (fig. S3I). Low levels of UGO-AID/HA did not allow its detection by Western blot or immunofluorescence assays to assess degradation of the protein upon addition of auxin to gametocytes. Addition of the AID/HA tag to the UGO C terminus also imposed a fitness cost, with low exflagellation rates even in the absence of auxin. However, addition of auxin for 1 hour before gametocyte activation led to a reduction in the formation of exflagellation centers (Fig. 3J), suggestive of UGO down-regulation. Consistent with this observation, induction of UGO-AID/HA depletion led to a 10-fold reduction in calcium mobilization upon stimulation by XA or a rise in pH (Fig. 3K and fig. S3J). However, in contrast to GCα, UGO-depleted gametocytes were still responsive to BIPPO. A similar pattern was observed for cGMP levels with UGO-depleted parasites showing elevated cGMP levels 20 s upon treatment with BIPPO but not with XA (Fig. 3L). These observations are important as they indicate that UGO is not

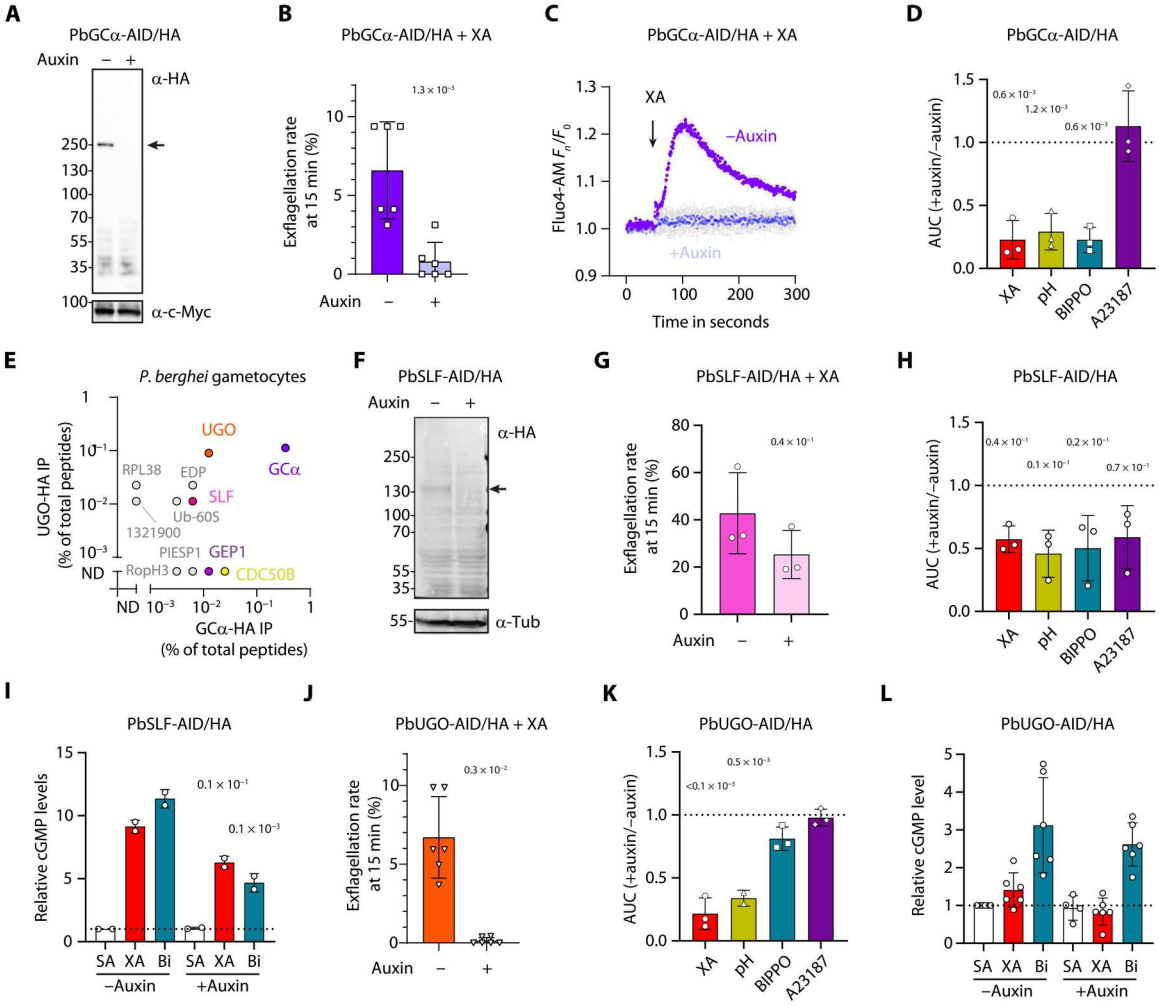

Fig. 3. In *P. berghei*, GCα is part of a signaling platform whose basal and induced activities are differentially regulated by SLF and UGO, respectively. (**A**) GCα-AID/HA is not detectable anymore after 1 hour of degradation with auxin. Tir1 is tagged by c-Myc and serves as a loading control. (**B**) A strong reduction of exflagellation in response to XA is observed upon GCα-AID/HA degradation (SD; $n = 6$ biological replicates, unpaired two-tailed t test). (**C**) Fluorescence kinetics of gametocytes upon GCα-AID/HA degradation in response to 100 μM XA. (**D**) The relative AUC of Fluo-4 AM fluorescence upon GCα degradation compared to untreated gametocytes (SD; $n = 3$ biological replicates, unpaired two-tailed t test). (**E**) Mass spectrometry identification of proteins immunoprecipitated (IP) from lysates of UGO-HA and GCα-HA gametocytes. ND, not detected ($n = 2$ biological replicates). (**F**) Depletion of SLF-AID/HA upon auxin treatment (expected size is 144 kDa). (**G**) A twofold reduction of exflagellation in response to XA is observed upon SLF-AID/HA degradation (SD; $n = 3$ biological replicates, unpaired two-tailed t test). (**H**) AUC of the fluorescence response upon SLF-AID/HA degradation compared to untreated gametocytes (SD; $n = 3$ biological replicates, unpaired two-tailed t test). (**I**) Relative basal and induced cGMP levels upon treatment with XA and BIPPO (Bi) in SLF-AID/HA gametocytes in presence or absence of IAA (SD; $n = 3$ biological replicates, one-way ANOVA). (**J**) A strong reduction of exflagellation in response to XA is observed upon UGO-AID/HA degradation (SD; $n = 6$ biological replicates, unpaired two-tailed t test). (**K**) AUC of the fluorescence response upon UGO degradation compared to untreated gametocytes (SD; $n = 3$ biological replicates, unpaired two-tailed t test). (**L**) Relative basal and induced cGMP levels upon treatment with XA and BIPPO in UGO-AID/HA gametocytes in presence or absence of auxin (SD; $n = 2$ biological replicates with technical duplicates, one-way ANOVA).

required for GCα, PDEα, and PDEδ basal activities but is essential to up-regulate GCα activity in response to XA or pH.

UGO is required for XA-mediated activation of gametogenesis in *P. falciparum*

We then wondered whether UGO is also required to control response to XA in *P. falciparum* gametocytes. To address this, we investigated the phenotypic consequences of *PfUGO* deletion (PF3D7_1003000). Because *PfUGO* was also predicted to be essential in *P. falciparum* (*44*), we opted to conditionally delete *PfUGO* using the rapamycin-inducible DiCre system (fig. S4A) (*45*). Generation of a marker-free *PfUGO-HA:cKO* line was achieved using a Cas9-mediated strategy. Briefly, a C-terminal triple HA tag and two *loxP* sites (one within the *2loxPint* and one downstream of the HA tag) were introduced to truncate the *PfUGO* gene upon DiCre-mediated recombination (fig. S4A). As in *P. berghei* gametocytes, the very low levels of protein expression prevented us from detecting the protein by immunofluorescence and Western blotting in dimethyl sulfoxide (DMSO)– or rapamycin-treated schizonts. However, immunopurification of PfUGO-HA recovered three peptides mapping on PfUGO, while no such peptides were detected in presence of rapamycin (table S2). Three GCα peptides were also

detected in PfUGO-HA immunoprecipitates only in absence of rapamycin. While it is not possible to assess the statistical significance of these differences, these observations suggest depletion of PfUGO-HA in presence of rapamycin as well as a conserved interaction between UGO and GCα in *P. falciparum* gametocytes.

We then monitored the development of *PfUGO-HA:cKO* gametocytes treated with DMSO (control) or rapamycin at the sexual ring stage. Knocking out *PfUGO* had no apparent effect on gametocyte maturation and did not also affect the gametocyte sex ratio, as monitored by the expression of Pfg377 (Fig. 4A and fig. S4B). This protein is known to be associated with osmiophilic bodies, which are mainly found in *P. falciparum* female gametocytes (*46*). In control gametocytes, stimulation by XA of stage V *PfUGO-HA:cKO* gametocytes led to the activation of female gametocytes, as assessed by surface expression of Pfs25 (Fig. 4B) (*47*). Similarly, activation by XA led to the formation of motile flagellated male gametes as assessed by the formation of exflagellation centers (Fig. 4C). However, *PfUGO* deletion led to a complete inhibition of female and male gametocyte activation (Fig. 4, B and C), confirming the essential role of PfUGO in the XA-dependent activation of gametogenesis in *P. falciparum*.

UGO and GCα coimmunoprecipitate in *P. berghei* schizonts

As GCα was previously shown to be essential for merozoite egress in *P. falciparum* (*25*) and for the proliferation of asexual blood stages in *P. berghei* (*48*) and *P. yoelii* (*26*), we wondered whether a conserved set of partners would be required to control its activity at this stages. To do so, we used affinity purification of 3xHA-tagged GCα and UGO from in vitro–cultured *P. berghei* schizonts under cross-linking conditions and combined label-free semiquantitative mass spectrometry to identify interacting proteins (Fig. 5A). As in gametocytes, we identified GCα, CDC50B, UGO, and SLF in both immunoprecipitates. We additionally detected at least two peptides mapping on 31 other proteins that correspond to exported or ribosomal proteins and likely represent unspecific interactions (table S1). The identification of GCα, CDC50B, UGO, and SLF in coimmunoprecipitates from different *Plasmodium* stages raised the intriguing possibility that a conserved signaling platform integrates different signals across the life cycle of malaria parasites.

PDE inhibition induces egress of *P. berghei* merozoites and identifies distinct requirements for UGO during schizogony and egress

Given the fact that, in *P. berghei* gametocytes, UGO is essential to up-regulate GCα activity in response to signals that are apparently specific to the mosquito environment, we wondered whether it would also be important to regulate GCα activity in *P. berghei* schizonts. However, *P. berghei* parasites develop normally into merozoites in in vitro culture but cannot egress from the erythrocyte without additional mechanical shear stress (*49*). As the GCα platform is conserved in *P. berghei* schizonts and artificial elevation of cGMP levels using PDE inhibition by zaprinast leads to *P. falciparum* egress, we asked whether PDE inhibition would also induce egress of *P. berghei* merozoites. We first monitored calcium mobilization in *P. berghei* schizonts following zaprinast, BIPPO, and A23187 treatments at 37°C. To ensure that the observed signals were not originating from contaminating gametocytes, we used the non–gametocyte-producing ANKA 2.33 (NGP) line (*50*). Response to the three molecules were similar to those observed in gametocytes (Fig. 5, B and C), suggesting that GCα also displays a basal activity that is counterbalanced by PDE activity in *P. berghei* schizonts. As zaprinast induced the strongest calcium response under our experimental conditions, we then counted in vitro–cultured schizonts following 50 min of DMSO or zaprinast treatment. Zaprinast led to a significant twofold reduction in schizont numbers (Fig. 5D), suggesting that zaprinast also stimulates the egress of *P. berghei* merozoites.

The possibility to induce *P. berghei* merozoite egress with zaprinast opened the possibility to investigate the role of UGO in zaprinast-induced egress. Addition of auxin at the onset of the schizont culture led to a significant 1.7-fold reduction in schizont numbers 50 min after zaprinast treatment. In contrast, addition of auxin to segmented UGO-AID/HA schizonts for 1 hour did not affect zaprinast-induced egress. These results suggest that UGO plays a role both to activate GCα basal activity during schizogony and to enhance its activity just before egress (Fig. 5E). However, the asynchronous in vivo growth of *P. berghei* asexual blood stages together with the absence of merozoite natural egress in vitro prevented us to further study the role of UGO in naturally induced egress in *P. berghei*.

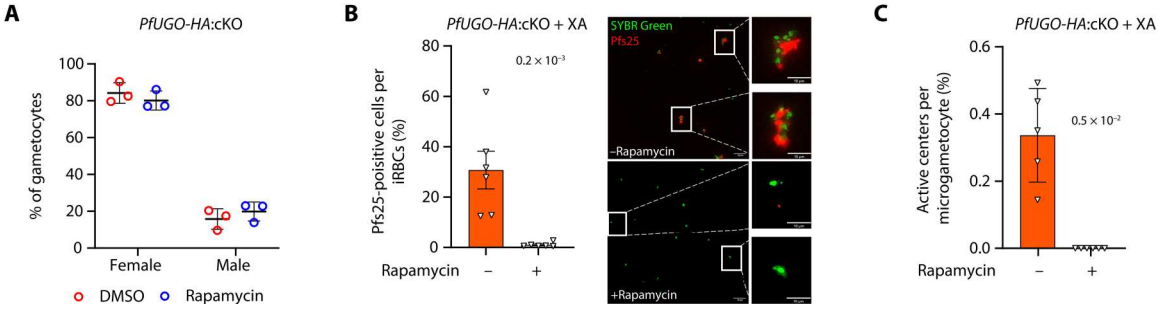

Fig. 4. UGO is essential for XA-dependent activation of gametogenesis in *P. falciparum*. Conditional deletion of *PfUGO* in sexual ring stages does not affect the sex ratio (**A**) but significantly affects female gametogenesis (**B**) and male gametogenesis (**C**) [SD; $n = 3$ (A) and $n = 5$ (B) and (C) biological replicates, unpaired two-tailed t test]. In (B), representative images from the fluorescence microscopy–based female gamete activation assay are shown. DMSO (top)– or rapamycin (bottom)–treated gametocytes were stained with SYBR Green and α-Pfs25 antibodies. Activated females form clusters of cells and are Pfs25-positives. Scale bars, 30 μm, insets 2 μm.

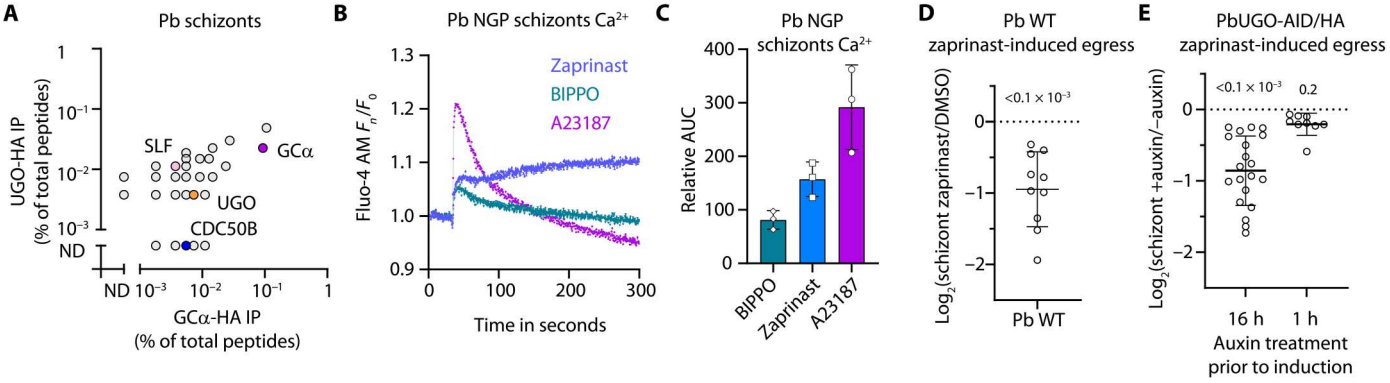

Fig. 5. UGO interacts with GCα in *P. berghei* schizonts and shows differential requirement for zaprinast-induced egress. (**A**) Mass spectrometric identification of proteins immunoprecipitated from lysates of UGO-HA and GCα-HA *P. berghei* schizonts ($n = 2$ biological replicates). (**B**) Fluorescence response kinetics of schizonts of the non–gametocyte-producing ANKA 2.33 (NGP) line loaded with Fluo-4 AM. Cells are stimulated with zaprinast, BIPPO, or A23187. (**C**) The relative AUC of Fluo-4 AM fluorescence upon stimulation. Error bars show SD from the mean from three independent infections. (**D**) Change in the numbers of schizonts, as assessed by Giemsa staining, following 50 min of treatment of cells with DMSO or zaprinast (SD; $n = 5$ independent inductions from two biological replicates, unpaired two-tailed *t* test). (**E**) Change in the numbers of schizonts, as assessed by Giemsa staining, following 50 min of treatment of cells with zaprinast upon UGO-AID/HA degradation at the onset of the culture (16 hours) or 1 hour before treatment (1 hour) [SD; $n = 5$ independent inductions from four biological replicates (16 hours) and two biological replicates (1 hour), unpaired two-tailed *t* test).

UGO is essential for natural egress and invasion but can be bypassed by PDE inhibition in *P. falciparum*

To further investigate the role of UGO in natural merozoite egress, we characterized the phenotypic consequences of *UGO* deletion during *P. falciparum* schizogony. *PfUGO* was conditionally deleted by adding rapamycin 2 hours after invasion on *PfUGO-HA:cKO* ring stages. As in *P. berghei* gametocytes and schizonts, the very low levels of protein expression prevented us from detecting the protein by immunofluorescence and Western blotting in DMSO- or rapamycin-treated schizonts. However, monitoring of DMSO- and rapamycin-treated *PfUGO-HA:cKO* parasites under shaking conditions showed no increase in parasitemia in the rapamycin-treated cultures (Fig. 6A). Rapamycin-treated parasites formed morphologically normal mature schizonts at the end of the erythrocytic cycle of treatment (cycle 0) as shown by fluorescence or electron microscopy (Fig. 6, B and C), indicating no detectable effects on intracellular development. However, very few schizonts from the rapamycin-treated cultures underwent egress (Fig. 6D and fig. S5A), resulting in a significant reduction in newly invaded rings (Fig. 6E), indicating that UGO is essential for natural egress of *P. falciparum* schizonts.

We then investigated whether *PfUGO*-deleted merozoites were capable of reinvasion following physical disruption of the blocked schizonts. To do so, segmented schizonts were agitated at 1500 rpm, and the number of schizonts, merozoites attached to a naïve erythrocyte, and ring stages were determined after 2 hours with the ImageStream system (Fig. 6F and fig. S5B). Agitation allowed to rupture 40 and 15% of *PfUGO-HA:cKO* schizonts in the absence or presence of rapamycin, respectively. In sister cultures that were not agitated, 20% of schizonts egressed in the absence of rapamycin, while no egress was observed for rapamycin-treated parasites (Fig. 6G). Under this experimental setup, conditional deletion of *PfUGO* led to a 25-fold decrease in the number of ring parasites per ruptured schizont (Fig. 6H), indicating that UGO is also required for merozoite invasion of erythrocytes.

We then set out to determine whether UGO is required for induced egress. It was previously shown that merozoite egress could be stimulated by PC in a protein phosphatase 1 (PP1)-dependent manner (*10*). However, PC did not induce merozoite egress in the presence or absence of UGO under our experimental settings (Fig. 6I and fig. S5C). We then tested whether *PfUGO* deletion could be bypassed in *P. falciparum* schizonts by artificial elevation of cGMP levels using PDE inhibition by zaprinast or BIPPO. We found 500 μM zaprinast to be more efficient than 5 μM BIPPO to activate calcium mobilization in WT schizonts (fig. S5D) and performed subsequent experiments with zaprinast only. *PfUGO*-null parasites exposed to 500 μM zaprinast egressed, as well as nonexcised schizonts (Fig. 6J). *PfUGO*-null schizonts also mobilized calcium in response to zaprinast (Fig. 6K). They however showed a slower mobilization of calcium compared with nontreated parasites. Following zaprinast-induced egress, resulting merozoites were able to reinvade naïve erythrocytes 15 min posttreatment (Fig. 6L). We also noticed a significant increase in ring formation following rapamycin treatment, which we attribute to a better synchronicity of induced egress in the absence of *PfUGO*. Together, these results suggest that, in *P. falciparum*, UGO is essential for natural merozoite egress and reinvasion by up-regulating the cGMP/Ca^{2+} pathway in response to currently unknown signals.

A decrease in the membrane tension of gametocytes correlates with UGO-dependent up-regulation of GCα

As UGO seems to be equally important to up-regulate GCα activity in *P. berghei* gametocytes and *P. falciparum* schizonts, we reasoned that XA could also stimulate egress in *P. falciparum* schizonts. However, exposure of segmented schizonts to 100 μM XA did not induce any significant increase of egress of *P. falciparum* merozoites nor calcium mobilization in *P. berghei* and *P. falciparum* schizonts compared to nontreated parasites (Fig. 6I and fig. S5D). We thus wondered how UGO could differentially integrate signals of various natures at a given stage or across stages. It is plausible that our interactome analysis may have missed stage- or signal-specific

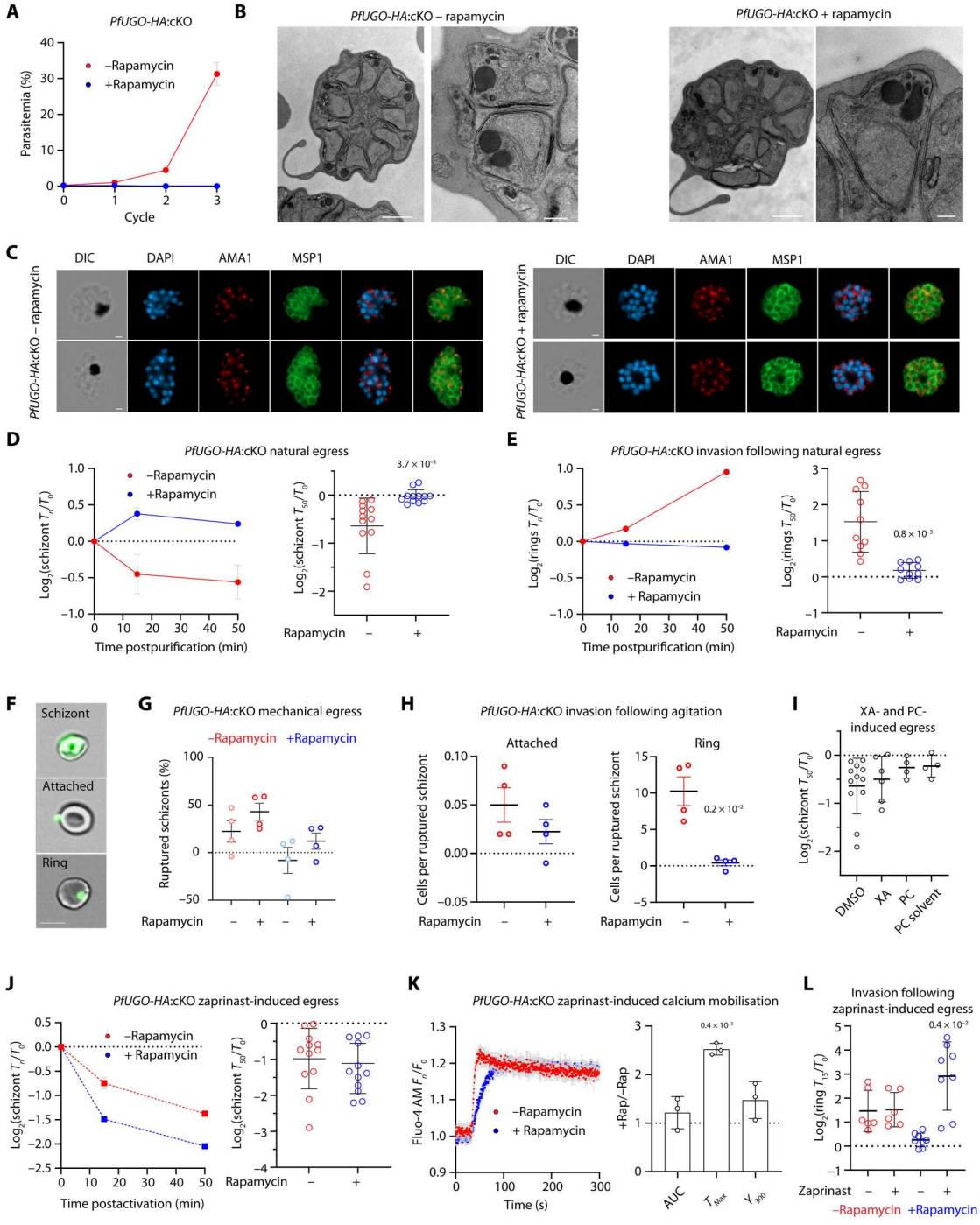

Fig. 6. UGO is essential for *P. falciparum* merozoite egress and invasion but can be bypassed by PDE inhibition. (**A**) Replication of DMSO- and rapamycin-treated *PfUGO-HA:cKO* parasites (SD; $n = 3$ independent infections). (**B** and **C**) *PfUGO*-deleted parasites reach late schizogony as observed by electron microscopy (B). Scale bars, 1 μm (left) and 200 nm (right). AMA1 and MSP1 localization by immunofluorescence (C). Scale bars, 2 μm. (**D**) Conditional deletion of *PfUGO* leads to the accumulation of schizonts (left: data from two sister cultures; right: replicates from six independent cultures; unpaired two-tailed *t* test). (**E**) Conditional deletion of *PfUGO* leads to a diminution of ring stage formation (left: duplicates from two sister cultures; right: replicates from five independent cultures; two-tailed *t* test). (**F**) Representative images used to quantify schizonts, attached merozoites, and ring stages. Bright-field and SYBR Green (green) channels are shown. Scale bar, 7 μm. (**G**) Agitation leads to the rupture of 19% of UGO-blocked schizonts ($n = 4$ biological replicates, unpaired two-tailed *t* test). (**H**) *PfUGO* conditional deletion reduces merozoite attachment and ring formation following mechanical disruption of schizonts ($n = 4$ biological replicates, unpaired two-tailed *t* test). (**I**) Treatment of *P. falciparum*–segmented schizonts with 100 μM XA or 50 μM PC treatments does not induce egress. (**J**) Treatment of segmented schizonts with the PDE inhibitor zaprinast bypasses the requirement of PfUGO for egress (left: data from two sister cultures; right: replicates from six independent cultures; unpaired two-tailed t test). (**K**) *PfUGO*-deleted schizonts are responsive to zaprinast (SD; left: $n = 3$ technical replicates; right: $n = 3$ biological replicates; unpaired two-tailed *t* test). (**L**) Invasion following zaprinast-induced egress is not affected (SD; $n = 3$ biological replicates with technical duplicates; one-way ANOVA).

protein components of the GCα platform. Alternatively, given that all identified components of the GCα platform are multipass membrane proteins, we hypothesized that intramembrane sensing could, in conjunction with stage-specific platform partners, be key to integrate various signals regulating GCα in a UGO-dependent manner. To test this hypothesis, we took advantage of the Flipper-TR fluorescent probe that specifically targets cell membranes and reports membrane tension changes through its fluorescence lifetime changes (*51*). This provided a unique opportunity to assess the general membrane tension of intracellular parasites in response to activating signals (Fig. 7, A and B). To allow imaging of a large number of cells in response to signals stimulating gametogenesis, we imaged the Flipper-TR probe in P_{ama1}ICM1 gametocytes that showed similar membrane tension compared with WT parasites (fig. S6). P_{ama1}ICM1 gametocytes are responsive to XA but blocked downstream of cGMP (*52*), allowing long-term imaging of membrane tension upon activation. XA or a rise in pH led to a significant decrease in the fluorescence lifetime of the probe, indicative of a decrease of membrane tension. Exposure of gametocytes to kynurenic acid, a XA-related metabolite lacking the hydroxyl group at the eight position of the quinoline ring, or the PDE inhibitor BIPPO did not lead to changes in the fluorescence lifetime of the Flipper-TR probe. Unexpectedly, XA and a rise in pH also significantly decreased the membrane tension of infected erythrocytes (Fig. 7C), while noninfected erythrocytes were not affected by these two factors (Fig. 7D). Lysis of the host erythrocyte membranes with saponin, as measured by the absorbance of hemoglobin at 414 nm (Fig. 7E) (*53*), did not differentially affect calcium response to XA compared to treatments with BIPPO or A23187 (Fig. 7F), suggesting that the plasma membrane of the infected erythrocyte is not essential to mediate XA stimulation. It was previously reported that approximately 70% of lipid classes exhibit a significant difference in abundance between *P. falciparum* asexual blood stages and gametocytes (*54*). We thus wondered whether these differences could possibly explain the differential sensing of XA by schizonts and gametocytes. In accordance with this hypothesis, we found that XA did not affect membrane tension of *P. falciparum* merozoites (Fig. 7, G and H). Together, these results provide preliminary evidence that changes in the tension of gametocyte membranes may be involved in the up-regulation of GCα in a UGO-dependent manner.

DISCUSSION

Malaria parasites show a remarkable life cycle with multiple cellular differentiation events that require tight regulation. For example, control over gametocyte activation or merozoite egress is crucial to avoid premature and abortive development. In vivo, efficient gametogenesis relies on a rise in pH and presence of XA at a permissive temperature (*55*). These environmental factors encountered in the mosquito midgut lead to elevated cGMP levels in the parasite

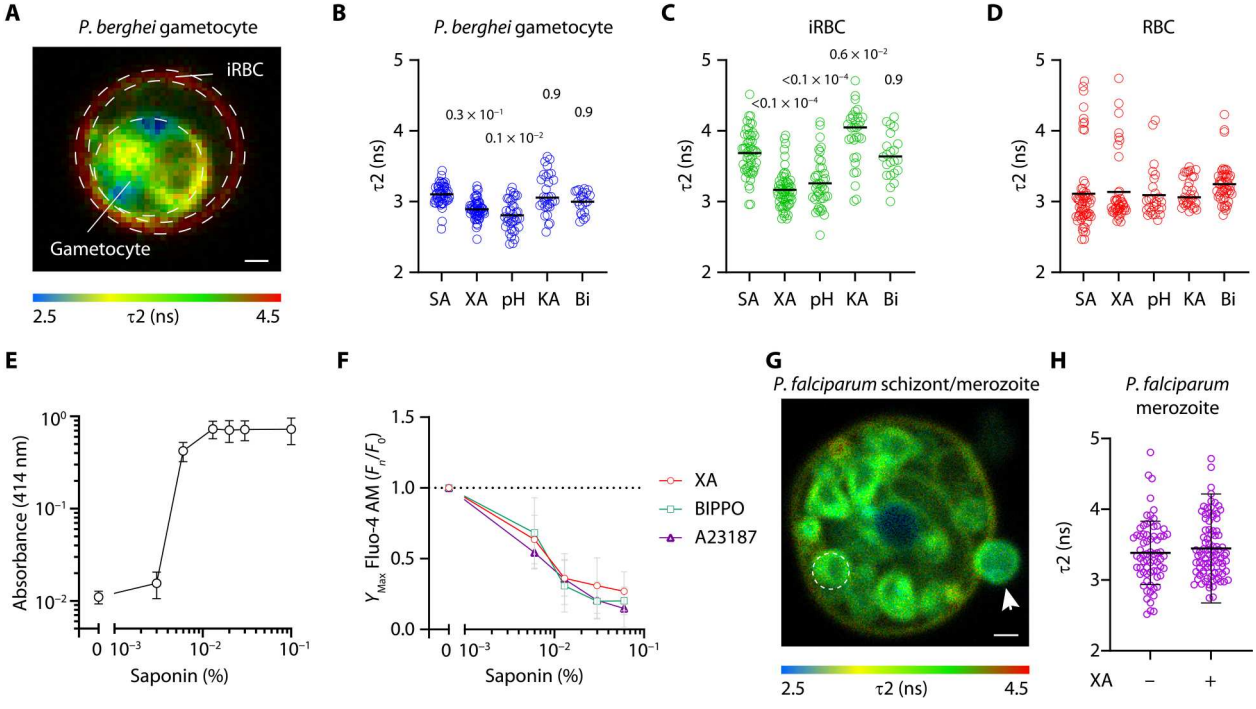

Fig. 7. XA and a rise in extracellular pH similarly lower membrane tension in gametocytes but not in schizonts. (**A**) Lifetime fluorescence in nanoseconds of the Flipper-TR probe in membranes of a *P. berghei* gametocyte in an erythrocyte. Dashed lines illustrate the regions of interest analyzed. Scale bar, 1 μm. (**B** to **D**) Lifetime fluorescence quantification of P_{ama1}ICM1 gametocytes (B), infected erythrocytes (C), and noninfected erythrocytes (D) in presence of SA (pH 7.2), XA (pH 7.2), SA (pH 7.8), KA (pH 7.2), and BIPPO [(Bi), pH 7.2]. Circles represent values from single cells from at least three independent infections; one-way ANOVA. (**E**) Hemoglobin release upon exposure of a *P. berghei*–infected RBC to increasing concentration of saponin as measured by absorbance at 414 nm (SD; $n = 3$ biological replicates). (**F**) No difference in maximum calcium mobilization (Y_{Max}) is observed upon treatment with XA, BIPPO, and A23187 at a given saponin concentration (SD; $n = 3$ biological replicates). (**G**) Lifetime fluorescence in nanoseconds of the Flipper-TR probe in membranes of a *P. falciparum* schizont in an erythrocyte and an extracellular merozoite (white arrow). Dashed lines illustrate the regions of interest analyzed. Scale bar, 1 μm. (**H**) Lifetime fluorescence quantification of *P. falciparum* schizonts in the absence or presence of XA. Circles represent values from singles cells from at least three independent infections.

that activate multiple calcium-dependent signaling pathways required for *Plasmodium* gametogenesis (*34*). However, the exact role of each GC and PDE in integrating the three known factors required for gametogenesis remained poorly understood (*33*).

Here, we first showed that a drop in temperature is not essential for gametocyte activation, as assessed by calcium mobilization, but is necessary to trigger DNA replication that is initiated by the calcium-dependent protein kinase 4 within seconds of calcium mobilization (*35*, *56*). Such a strong block in DNA replication at 37°C is unexpected given that *Plasmodium* parasites are well adapted to replicate DNA at 37°C in their vertebrate host. The factor(s) limiting DNA replication at 37°C in gametocytes thus remain unknown. PDEα showed a relative decrease in activity at 20°C but is complemented by PDEδ that shows activity at both 37° and 20°C. It is thus possible that in vivo, a decrease in temperature may synergize with XA and pH to activate gametocytes. However, as deletion or inhibition of PDEs does not affect gametogenesis, this confirms that their main role in gametocytes is to prevent premature activation at 37°C in the mammalian host but not to respond to XA or pH (Fig. 8).

We thus turned our attention to the regulation of gametocyte activation by cGMP synthesis in response to XA and pH. GCα-depleted gametocytes were unresponsive to PDE inhibitors, indicating that GCα is the main active GC in gametocytes. The identification of GEP1 as a GCα interactor necessary for its basal cGMP synthesis activity in *P. yoelii* gametocytes (*26*) suggested that GCα is part of a signaling platform where GC activity may depend on cofactors, as previously shown in *T. gondii* (*41*). Here, we show that GCα interacts at least with three other multipass membrane proteins in *Plasmodium* gametocytes and schizonts: CDC50B, SLF, and UGO. Deletion of *CDC50B* does not impair asexual blood stages or gametogenesis. However, two other CDC50 proteins are encoded by *Plasmodium*, and it is possible that deletion of *CDC50B* is complemented by another CDC50 protein as suggested in (*39*). In support of this hypothesis, it was recently shown in *T. gondii* that multiple CDC50 proteins interact with the same P4-ATPase (*57*). We also showed that SLF is essential for growth of asexual blood stages and important for gametogenesis. This requirement is likely explained by SLF-dependent regulation of GCα basal activity. The depletion of SLF also affected calcium response to A23187, as previously observed in *T. gondii* (*42*, *43*), suggesting that SLF may also be more directly involved in the regulation of calcium homeostasis.

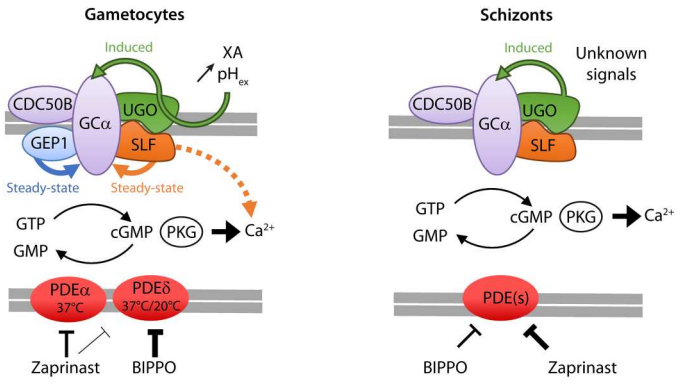

Fig. 8. Current model showing how cGMP homeostasis is regulated in *P. berghei* gametocytes and *P. falciparum* schizonts. In gametocytes (left), cGMP synthesis depends on GCα whose steady-state activity requires GEP1 and SLF. UGO induces GCα activity in response to XA or a rise in extracellular pH (pH_{ex}) possibly via lowered membrane tension. In nonactivated gametocytes, cGMP hydrolysis depends at least on PDEα and PDEδ that are both active at 37°C. PDEδ is also active at 20°C and dampens the induced signal. PDEα is targeted by zaprinast, and PDEδ is the main target of BIPPO in gametocytes. In schizonts (right), the same architecture is conserved, where UGO also induces GCα activity in response to unknown signals. Unidentified zaprinast- and BIPPO-sensitive PDEs prevent premature egress.

We found that conditional deletion of *PfUGO* and conditional depletion of UGO-AID/HA in *P. berghei* parasites blocked activation of naturally induced egress and gametogenesis. However, these phenotypes could be bypassed by artificial elevation of cGMP levels using PDE inhibitors. These results indicate that UGO is not required to maintain GCα basal activity but essential for induced GCα activity both in *P. falciparum* gametocytes and schizonts and in *P. berghei* gametocytes. In *P. berghei* schizonts, conditional depletion of UGO-AID/HA however led to distinct phenotypes: Early depletion led to a reduction in zaprinast-induced egress, while a late depletion had no significant effect. This suggests that the timing of UGO depletion or deletion highlights different requirements of UGO for GCα basal or induced activity. Consistent with this possibility, we previously showed that, in *T. gondii*, TgUGO also interacts with the unique TgGC and depletion of TgUGO-AID/HA over multiple rounds of parasite replication impaired TgGC basal activity. These observations suggest that UGO may have a dual function with requirement both for the activation of GCα basal activity via possibly its cellular trafficking or folding and for the GCα up-regulation in response to natural signals triggering merozoite egress and gametogenesis. Together, the conserved interaction between UGO, SLF, and GC in *Toxoplasma* tachyzoites and in *Plasmodium* schizonts and gametocytes suggests that the same membrane signaling platform is at play to regulate GC activity across the phylum of Apicomplexa. This casts a new light on how the regulation of this family of atypical GCs in response to multiple environmental signals requires a panel of cofactors.

The presence of a conserved CDC50/GC/UGO/SLF signaling platform across these three different forms of parasites suggests that UGO is not a direct sensor of both XA and pH. XA is not known to be involved in tachyzoite or merozoite egress, which we confirm here. However, acidification of the parasitophorous vacuole was previously shown to induce tachyzoite egress (*58*). It thus remains uncertain whether stage-specific components of the CDC50/GCα/UGO/SLF platform may be at play to integrate different signals across different parasites. Another GCα-interacting protein, GEP1, was previously shown to be only expressed in *Plasmodium* gametocyte and deletion of its coding gene was associated with the abolition of GCα basal activity (*26*). It was recently predicted that GEP1 may interact with XA and could represent the elusive XA sensor (*59*). However, the physiological relevance of this prediction in the activation of *Plasmodium* gametogenesis remains to experimentally established. Similarly, how elevation of the extracellular pH affects the activity of the CDC50/GEP1/GCα/UGO/SLF platform in gametocytes remains elusive. Here, we found that XA and pH lower membrane tension of *P. berghei* gametocytes, suggesting that the stage specificity of XA may be linked not only to the expression of a receptor in gametocytes but also to the specific properties of the membranes hosting the CDC50/GCα/UGO/SLF signaling platform. Consistent with this hypothesis, in

T. gondii tachyzoites, induction of GC-dependent egress requires production of phosphatidic acid in the external leaflet of the plasma membrane hosting TgGC (*41*). So far, we have not been able to confidently localize UGO in gametocytes and merozoites. Previous reports have indicated that GCα localizes to cytoplasmic vesicular structures in newly formed merozoites (*25*) and to cytoplasmic puncta in *P. yoelii* gametocytes (*26*). It is thus possible that UGO shows a similar localization in both stages, but more work will be required to define the exact membrane structure(s) hosting this signaling platform in *Plasmodium* and whether their lipid composition affects its regulation.

Together, our work and previous results highlight that a *Plasmodium* GCα membrane receptor platform integrates signals that are critical for natural merozoite egress, merozoite invasion, and gametocyte activation (Fig. 8). CDC50B is likely involved in GCα folding or trafficking during both stages but its deletion is possibly complemented by another CDC50 protein (*39*). GEP1 is only expressed in gametocytes where it is essential for GCα basal activity (*26*). SLF interacts with GCα in both schizonts and gametocytes, where it is important for its basal activity. Last, UGO is essential to enhance GCα activity in both schizonts and gametocytes. In schizonts, the natural signals inducing UGO-dependent activation of GCα remain to be identified. In gametocytes, we showed that UGO transduces XA and a rise in extracellular pH, two distinct signals that similarly reduce the membrane tension of gametocytes. As XA does not induce merozoite egress or decrease in schizont membrane tension, this highlights the membrane as a possible key player in GCα- and UGO-dependent sensing of signals inducing merozoite egress and gametocyte activation.

METHODS

Ethics statement

All animal experiments performed in Switzerland were conducted with authorization numbers GE/82/15 and GE/201/17, according to the guidelines and regulations issued by the Swiss Federal Veterinary Office.

Generation of DNA-targeting constructs

The oligonucleotides used to generate and genotype the mutant parasite lines are in table S3.

Restriction/ligation cloning, P. berghei

The gene deletion–targeting vector for *pde*α was constructed using the pAB022 plasmid, which contains polylinker sites flanking an *hdhfr* expression cassette conferring resistance to pyrimethamine. Polymerase chain reaction (PCR) primers MB763 and MB764 were used to generate a fragment of *pde*α 5′ upstream sequence from genomic DNA, which was inserted into Hind III and Pst I restriction sites upstream of the *hdhfr* cassette. A fragment generated with primers MB765 and MB766 from the 3′ flanking region of *pde*α was then inserted downstream of the *hdhfr* cassette using Kpn I and Not I restriction sites. The linear targeting sequence was released using Hind III and Not I, and the construct was transfected into the ANKA line 2.34 or PDEδ-KO. A schematic representation of the endogenous *pde*α, the constructs, and the recombined locus is in figs. S2 and S3.

PlasmoGEM vectors

3xHA, KO, or AID/HA tagging of GCα, UGO, and PDEγ was generated using phage recombineering in *Escherichia coli* TSA strain with PlasmoGEM vectors (https://plasmogem.umu.se/pbgem/). For final targeting vectors not available in the PlasmoGEM repository, generation of KO and tagging constructs was performed using sequential recombineering and gateway steps as previously described (*60*, *61*). For each gene of interest (goi), the Zeocin resistance/Phe sensitivity cassette was introduced using oligonucleotides goi HA-F × goi HA-R and goi KO-F × goi KO-R for 3xHA, AID/HA tagging, and KO targeting vectors. Insertion of the gateway (GW) cassette following gateway reaction was confirmed using primer pairs GW1 × goi QCR1 and GW2 × goi QCR2. The modified library inserts were then released from the plasmid backbone using Not I. The UGO-AID/HA and GCα-AID/HA targeting vectors were transfected into the 615 parasite line (*37*), and the PDEγ-KO, UGO-3xHA, and GCα-3xHA vectors into the 2.34 line. Schematic representations of the targeting constructs as well as WT and recombined loci are shown in figs. S1 to S6.

Restriction/ligation cloning, P. falciparum

The endogenous *PfUGO* locus in the p230p DiCre-expressing *P. falciparum* clone was modified using Cas9-mediated genome editing to generate the *PfUGO-HA*:cKO p230p DiCre parasite line using the plasmid pUC57 vector containing the following: (i) a 5′ homology region 1 (HR1) of 412 base pairs (bp) and (ii) a recodonized *PfUGO* sequence with a *loxpint* module fused to a triple HA epitope followed by a second *loxp* site that was synthesized. A 3′ HR2 of 624 bp amplified with primers *pfugo* HR2 forward and *pfugo* HR2 reverse was further cloned following Xho I digestion (data S1). The final targeting plasmid was linearized with Nco I-HF and Xho I overnight before transfection. To target the *PfUGO* locus, two guide RNA–encoding sequences were independently inserted into the pDC2-Cas9-hDHFR (human dihydrofolate reductase)/yFCU (yeast cytosine deaminase/uridyl phosphoribosyl transferase–containing plasmid) (*62*) using primer pairs *pfugo* grna F1/2 × *pfugo* grna R1/2. Constructs were transfected into the *P. falciparum* 3D7 p230pDiCre II-3 line (*62*).

P. berghei maintenance and transfection

P. berghei ANKA strain (*63*)–derived clones 2.34 (*35*) and 615 (*37*), together with derived transgenic lines, were grown and maintained in CD1 outbred mice. Six- to 10-week-old mice were obtained from Charles River Laboratories, and females were used for all experiments. Mice were specific pathogen–free (including *Mycoplasma pulmonis*) and subjected to regular pathogen monitoring by sentinel screening. They were housed in individually ventilated cages furnished with a cardboard mouse house and Nestlet, maintained at 21° ± 2°C under a 12-hour light/12-hour dark cycle, and given commercially prepared autoclaved dry rodent diet and water ad libitum. The parasitemia of infected animals was determined by microscopy of methanol-fixed and Giemsa-stained thin blood smears.

For gametocyte production, parasites were grown in mice that had been phenyl hydrazine–treated 3 days before infection. One day after infection by 0.5×10^7 to 1.5×10^7 parasites, sulfadiazine (20 mg/liter) was added in the drinking water to eliminate asexually replicating parasites. Microgametocyte exflagellation was measured 3 or 4 days after infection by adding 4 μl of blood from a superficial tail vein to 70 μl of exflagellation medium [RPMI 1640 containing 25 mM Hepes, 4 mM sodium bicarbonate, 5% fetal calf serum (FCS), and 100 μM XA (pH 7.4)]. To calculate the number of exflagellation centers per 100 microgametocytes, the percentage of RBCs

infected with microgametocytes was assessed on Giemsa-stained smears. For gametocyte purification, parasites were harvested in SA medium [RPMI 1640 containing 25 mM Hepes, 5% FCS, and 4 mM sodium bicarbonate (pH 7.20)] and separated from uninfected erythrocytes on a Histodenz cushion made from 48% Histodenz stock [27.6% (w/v) Histodenz (Sigma-Aldrich) in 5.0 mM tris-HCl, 3.0 mM KCl, and 0.3 mM EDTA (pH 7.20)] and 52% SA, with a final pH of 7.2. Gametocytes were harvested from the interface. To induce degradation of AID/HA-tagged proteins, 1 mM auxin dissolved in ethanol (0.2% final concentration) was added to parasites for 1 hour before activation.

Schizonts for transfection were purified from overnight in vitro culture on a Histodenz cushion made from 55% Histodenz stock and 45% phosphate-buffered saline (PBS). Parasites were harvested from the interface and collected by centrifugation at 500*g* for 3 min, resuspended in 25 µl of the Amaxa Basic Parasite Nucleofector solution (Lonza), and added to 10 to 20 µg of DNA dissolved in 10 µl of H_2O. Cells were electroporated using the FI-115 program of the Amaxa Nucleofector 4D. Transfected parasites were resuspended in 200 µl of fresh RBCs and injected intraperitoneally into mice. Parasite selection with pyrimethamine (0.07 mg/ml; Sigma-Aldrich) in the drinking water (pH ~ 4.5) was initiated 1 day after infection. Each mutant parasite was genotyped by PCR using three combinations of primers, specific for either the WT or the modified locus on both sides of the targeted region (experimental designs are shown in figs. S1 to S6). For allelic replacements, sequences were confirmed by Sanger sequencing using the indicated primers. Controls using WT DNA were included in each genotyping experiment; parasite lines were cloned when indicated.

Zaprinast-induced egress of *P. berghei* schizonts

Schizonts were cultured in vitro overnight as described above. For egress assays using the UGO-AID/HA line, cultures were divided into two, and 1 mM auxin or 0.2% ethanol was added to the culture medium 16 or 1 hour before start of the egress assay, respectively. For each biological replicate, 500-µl samples of each culture were transferred into five microfuge tubes for each tested condition and incubated with 500 µM zaprinast or 4% DMSO for 50 min at 37°C for 600 rpm. Egress efficiency was assessed from methanol-fixed and Giemsa-stained thin blood smears by determining numbers of schizonts per numbers of RBCs in a blinded manner.

Flow cytometry analysis of *P. berghei* gametocyte DNA content

DNA content of microgametocytes was determined by flow cytometry measurement of fluorescence intensity of cells stained with Vybrant dye cycle violet (Life Technologies) as previously described (*56*). Gametocytes were purified and resuspended in 100 µl of SA. Activation was induced by adding 100 µl of modified exflagellation medium [RPMI 1640 containing 25 mM Hepes, 4 mM sodium bicarbonate, 5% FCS, and 200 µM XA (final pH 7.8)]. To rapidly block gametogony, 800 µl of ice-cold PBS was added and cells were stained for 30 min at 4°C with Vybrant dye cycle violet and analyzed using a Beckman Coulter Gallios 4. Gating was performed on both micro- and macrogametocytes, and cell ploidy was expressed as a percentage of all gametocytes. For each sample, >5000 cells were analyzed.

Measurement of intracellular cGMP levels

To measure relative intracellular cGMP levels, *P. berghei* gametocytes were purified as described above and, for AID/HA lines, incubated with auxin or DMSO for 1 hour at 37°C. Samples were then treated with XA or BIPPO for 20 s and flash-frozen in liquid nitrogen before thawing on ice and lysis in presence of 200 µl of 0.1 M HCl for 10 to 20 million parasites per sample. Samples were then frozen and thawed two more times with intermittent vortexing. Intracellular cGMP levels were measured using the Direct cGMP enzyme-linked immunosorbent assay kit (Enzo Life Sciences) using the acetylation protocol to increase sensitivity. Standards were fitted to a sigmoidal curve and used to determine cGMP concentrations in the samples.

P. falciparum maintenance, synchronization, and transfection

Lines were maintained at 37°C in human RBCs in complete RPMI 1640 (Gibco, lot 2436708) containing 10% human ammonium bicarbonate (AB) serum (Macopharma, MDV 7000LA). Cultures were routinely microscopically examined using Giemsa-stained thin blood films. To obtain highly synchronized parasites, mature schizonts were isolated by centrifugation over 70% (v/v) isotonic Percoll (GE Healthcare, Life Sciences) cushions and cultured in fresh RBCs for 2 hours to allow rupture and reinvasion before removal of unruptured schizonts using 5% D-sorbitol for 8 min at 37°C (Sigma-Aldrich, #SLBJ4425V).

For transfection, purified schizonts were electroporated with 40 µg of circular plasmid DNA using the Amaxa Nucleofactor 4D (Lonza) and Nucleofector Kits for Parasites (Lonza). Parasites containing the integrated plasmid were selected by drug cycling in the presence of 2.5 nM WR99210 (Jacobus Pharmaceuticals, Princeton, NJ, USA) and then cloned by limiting dilution. Clonal transgenic lines were obtained by serial limiting dilution in flat-bottomed 96-well plates followed by selection of single plaques. For parasite genomic DNA extraction, the QIAGEN DNeasy Blood and Tissue kit was used. Genotype analysis PCR was done using the GoTaq (Promega) DNA master mix. DiCre activity was induced by rapamycin treatment of early rings (2 to 3 hours after invasion) as previously described (*64*). Samples for excision PCRs were collected 24 hours after rapamycin treatment.

Synchronous ring-stage parasites (2 to 3 hours postinvasion) at 0.1% parasitemia in 5% hematocrit were dispensed in triplicates into a six-well plate. DiCre-mediated excision of DNA was induced by transient rapamycin treatment. Five microliters from each well was sampled at 0, 2, 4, and 6 days and microscopically examined using Giemsa-stained thin blood films. Parasitemia was calculated at each time point by choosing randomly 10 to 12 microscopic fields as follows: number of infected RBCs/total number of RBCs × 100.

P. falciparum induction of gametocytogenesis and gametocyte culture

Parasites were cultured in complete media [25 mM Hepes (pH 6.72), 100 mM hypoxanthine, 24 mM sodium bicarbonate 0.5% Albumax II, 2 mM choline chloride, and neomycin (0.1 g/liter)] and synchronized as rings with sorbitol as described above for three consecutive days, reaching a final parasitemia between 1 and 3% in 5% hematocrit. Old rings/young trophozoites were induced using minimal fatty acid medium [RMPI/Hepes complemented

with 3.6% $NaHCO_3$, 100 mM hypoxanthine, bovine serum albumin (BSA; 390 mg/100 ml), 30 μM oleic acid, and 30 μM palmitic acid]. One day after induction, schizonts/young ring parasites were fed with serum medium [25 mM Hepes, 100 mM hypoxanthine, 24 mM sodium bicarbonate, 10% human AB serum, and neomycin (0.1 g/liter)] and treated with rapamycin (0.1 μM) or DMSO for 48 hours. Twenty-four hours later [gametocyte day 1 (Gamday1)], parasites were fed with serum/*N*-acetylglucosamine (GlucNac) medium (serum medium complemented with 50 mM GlucNac) for seven consecutive days to eliminate asexual parasites (*65*). Parasites were cultured in a heating plate from Gamday6 onward to ensure the maintenance of 37°C. On day 8, parasites were fed with serum medium and kept until day 13 (gametocyte stage V) when exflagellation and female activation assays were performed.

Sex ratio determination by immunofluorescence microscopy of *P. falciparum* gametocytes

Exflagellation assays were performed as described previously (*66*) with minor modifications. Thin smears were made by harvesting 500 μl of gametocyte cultures (Gamday10), spinning them down (400*g*, 1 min), and washing them with PBS 1×. Immunofluorescence assay (IFA) slides were fixed with 60% methanol/40% acetone (at −20°C) for 3 min. Slides were stored at −80°C until the next day. Slides were air-dried and wells were marked with a hydrophobic pen. Cells were hydrated with PBS 1× and blocked with 3% BSA in PBS 1× for 1 hour. Primary antibodies were added (1:1000; rabbit anti-Pfg377) (*67*) and incubated for 1 hour. After washing six times with PBS 1×, secondary (1:250; anti-rabbit 568) antibodies were incubated for 1 hour in the dark. Washes were performed as before. The antifade agent (Vectashield) supplemented with the fluorescent DNA stain 4′,6-diamidino-2-phenylindole (DAPI) (1 μg/ml) was added to each well, and the slides were sealed. Analyses were performed using a fluorescence microscope Leica DM 5000B using the ×40 objective. Around 200 to 300 DAPI-positive cells were counted per condition.

P. falciparum exflagellation assays

Giemsa smears of gametocyte day 13 cultures were made to determine the gametocytemia: 500 μl of each culture was taken and centrifuged 300*g* for 30 s, and 2 μl of the pellet was resuspended in 50 μl of 1× exflagellation medium (serum medium containing 100 μM XA). The activation mix was incubated in a Neubauer chamber in the dark in a humid chamber for 15 min. Exflagellation centers were counted, as well as the cell density. The percentage of exflagellating gametocytes was calculated as follows

$$\frac{\text{average of exflagellation centers}}{\text{gametocyteamia} \times \text{cell density}} \times 100$$

P. falciparum female gamete activation assay

Female activation assays were performed as described previously (*68*). Briefly, 250 μl of gametocyte culture was taken and centrifuged 300*g* for 30 s. The pellet of infected RBCs was resuspended in an activation medium containing 100 μM XA, mouse anti-PfS25 (1:2000) primary antibodies (*47*), and anti-mouse Alexa Fluor 594 (1:250) secondary antibodies. Samples were incubated overnight, under rotation, in the dark at room temperature. SYBR Green (1:10,000) was added and incubated at room temperature for 30 min in the dark. After spinning down and washing with PBS 1×, the samples were resuspended in 250 μl of PBS 1×. Parasites were plated in a black Greiner-CELLSTAR 96-well plate (Greiner, 655090; poly-D-lysine, flat μClear bottom) to get 0.05% hematocrit in each well. The plates were analyzed using an ImageXpress Micro wide-field high-content screening system (Molecular Devices) in combination with the MetaXpress software (version 6.5.4.532; Molecular Devices) equipped with a Sola SE solid-state white light engine (Lumencor), in combination with the MetaXpress software (version 6.5.4.532; Molecular Devices). Filter sets for SYBR Green [excitation (Ex): 472/30 nm, emission (Em): 520/35 nm] and Alexa Fluor 594 (Ex: 562/40 nm, Em: 624/40 nm) were used with exposure times of 40 and 50 ms, respectively; 121 sites per well were imaged using a Plan-Apochromat ×40 objective (Molecular Devices, catalog no. 1-6300-0412). Automated image analysis was performed as described in table S4.

Immunofluorescence assays

Following schizont purification, parasites were fixed in 4% paraformaldehyde and washed. After letting samples to adhere in a poly-D-lysine–covered slide, cells were permeabilized with 0.2% Triton X-100, followed by washes with PBS 1×, and incubation with a 2% BSA blocking solution in 1× PBS for 30 min. Samples were incubated with anti-AMA1 monoclonal antibody (mAb) (1:50; rabbit) and anti-MSP1.19 mAb (1:1000; mouse) overnight at 4°C, following incubation with secondary antibodies anti-rabbit 594 and anti-mouse 488 (1:1000). Slides are mounted in mounting media containing DAPI (Vectashield with DAPI, reference H-1200).

Electron microscopy

Sample preparation and imaging were performed as previously described (*69*). RBCs infected with *P. falciparum* schizonts were fixed with 2.5% glutaraldehyde (Electron Microscopy Sciences) and 2.0% paraformaldehyde (Electron Microscopy Sciences) in 10 mM PBS (pH 7.4) for 1 hour at room temperature. Pelleted cells were embedded in 3% low melted agarose (Eurobio) in 10 mM PBS and dissected in small pieces for easier handling and to prevent loss of cells during subsequent processing steps. After extensive washing (5 × 5 min) in 0.1 M sodium cacodylate buffer (pH 7.4) (Sigma-Aldrich), samples were postfixed with 1% osmium tetroxide (Electron Microscopy Sciences) reduced with 1.5% ferrocyanide (Sigma-Aldrich) in 0.1 M sodium cacodylate buffer (pH 7.4) for 1 hour at room temperature, followed by postfixation with 1% osmium tetroxide alone (Electron Microscopy Sciences) in 0.1 M sodium cacodylate buffer (pH 7.4) for 1 hour at room temperature. After washing with double distilled water (2 × 5 min), samples were en block poststained with 1% aqueous uranyl acetate (Electron Microscopy Sciences) for 1 hour at room temperature. Samples were then washed with double distilled water for 5 min and dehydrated in graded ethanol series (2 × 50%, 1 × 70%, 1 × 90%, 1 × 95%, and 2 × 100% for 3 min each wash). Samples were then infiltrated at room temperature with Durcupan resin (Sigma-Aldrich) mixed 100% ethanol at 1:2, 1:1, and 2:1 for 30 min each step, followed by fresh pure Durcupan resin for 2 × 30 min and transferred into fresh pure Durcupan resin for 2 hours. Last, samples were embedded in fresh Durcupan resin filled small thin-wall PCR tubes and polymerized and cured at 60°C for 24 hours. Ultrathin sections (60 nm) were cut with a Leica Ultracut UCT microtome (Leica Microsystems) and diamond knife (DiATOME) and collected onto 2-mm single-

slot copper grids (Electron Microscopy Sciences) coated with 1% Pioloform plastic support film. Sections were then examined, and transmission electron microscopy (TEM) images were collected using a Tecnai 20 TEM (FEI) electron microscope operating at 80 kV and equipped with a side-mounted MegaView III charge-coupled device camera (Olympus Soft-Imaging Systems) controlled by iTEM acquisition software (Olympus Soft-Imaging Systems).

P. falciparum egress time course assays

Cultures of highly synchronous early ring-stage parasites (2 to 3 hours postinvasion) at 2% parasitemia in 5% hematocrit were cultured and split in two subcultures, one of each was treated with rapamycin, allowing the DiCre-mediated excision of DNA, while the other was treated with the rapamycin vehicle (0.1% DMSO). After reaching late schizogony, Percoll-enriched schizonts were resuspended in 500 μl of complete RPMI. After adding 5 μl of blood, the resuspended cultures were plated in a 96-well plate in triplicates (4×10^5 parasites per well) and challenged with either DMSO (1:33), zaprinast (500 μM), XA (100 μM), PC (50 μM) or PC solvent (water: ethanol:methanol; 1:1:2) for 0, 15, and 50 min at 37°C. Samples were collected and washed with PBS and fixed in 4% paraformaldehyde (AppliChem, A3813, 1000) and 0.0065% glutaraldehyde (Sigma-Aldrich, G5882) for 30 min at room temperature under rotation. After fixation, samples were washed twice with PBS and resuspended in PBS. Samples were stained with SYBR Green I nucleic acid gel stain (Thermo Fisher Scientific, catalog no. S7563) (diluted 1:20,000) and analyzed by with a Attune NxT flow cytometer using the Attune TM NxT Software; 15,000 events were recorded per sample. All flow cytometry data were analyzed with FlowJo software. To assess egress, we calculated the binary logarithm of the ratio of the percentage of schizonts from time n to 0 min: $\log_2 (t_n/t_0)$.

Multispectral imaging flow cytometry (ImageStreamX) analysis

Samples were run in a two-camera, 12-channel ImageStreamX multispectral imaging flow cytometer (Luminex Corporation) at low speed and highest magnification (×60). Instrument setup and performance tracking were performed daily using the Amnis SpeedBead Kit (Luminex Corporation) for verifying optimal instrument performance. Cells were excited using a 488-nm laser (15 mW) and a 785-nm side scatter (SSC) laser (1.5 mW). Only events with a bright-field (BF) area greater than 1 μm^2 (to exclude cell debris) and nonsaturating pixels were collected. Data were acquired for 50,000 events per sample. Panel experimental samples contained images and data for BF (channels 1 and 9), SYBR Green (channel 2; 480 to 560 nm), and SSC (channel 12; 745 to 800 nm). Data analysis was done using IDEAS software (version 6.2; Luminex). Cells were gated for the gradient RMS (root mean square) of the BF channel to exclude the out-of-focus events. Single cells are then located by plotting the area of the BF image versus the aspect ratio (the ratio of the width and height of the object, i.e., the shape) of the BF channel (channel 1). A region larger than 1 μm^2 of BF area was created to include free parasites. Events with lower aspect ratio and area larger than 90 μm^2 were excluded (doublets and aggregates). By plotting the intensity of SSC (X axis) versus the intensity of the SYBR Green (Y axis), five populations were obtained: schizonts, free merozoites, RBCs infected with one parasite, RBCs infected with two or more parasites, and uninfected RBCs. Because the RBCs infected with one parasite population is of interest for this study, this population was gated using the area of the BF channel versus the aspect ratio of the BF channel to exclude other cell debris. The bright spots of parasites were detected by plotting the intensity and the max pixel of the SYBR Green channel. Internalization was then measured by a score, which is defined by the ratio of the SYBR Green intensity inside the cell compared to the intensity of the entire cell (defined as the BF image). Cells with internalized objects have positive scores, while cells with no internalization are negative.

Calcium measurements

P. berghei and P. falciparum Fluo-4 AM calcium assays

To measure changes in calcium level, *P. berghei* gametocytes were harvested in coelenterazine loading buffer [CLB; PBS containing 20 mM Hepes, 20 mM glucose, 4 mM $NaHCO_3$, 1 mM EDTA, and 0.1% BSA (pH 7.2) (*35*). *P. berghei* gametocytes and schizonts and *P. falciparum* schizonts were purified as described above and resuspended in 1 ml and 500 μl of CLB, respectively, as well as loaded with 5 μM of Fluo-4 AM for an hour. The parasites were then washed twice with CLB and resuspended in 500 and 20 μl of this suspension that were added per well in a 96-well plate. Compound dispensing and simultaneous fluorescence reading were performed using FDSS μCELL (Hamamatsu Photonics) for a period of 5 min. The fluorescence value of each time point was first normalized to the initial fluorescence value at 0 s ($F_{t=n}/F_{t=0}$) and then by the vehicle control: $(F_{t=n}/F_{t=0})/(F\text{vehicle}_{t=n}/F\text{vehicle}_{t=0})$. As the relative fluorescence values vary from day to day, each experiment was normalized to a control (WT or noninduced) prepared on the same day.

P. berghei GFPaequorin calcium assays

Aequorin reconstitution and luminometric Ca^{2+} detection from purified *P. berghei* gametocytes were performed as previously described (*35*) with some modifications. First, purified gametocytes were washed three times in CLB [PBS, 20 mM Hepes, 20 mM glucose, 4 mM sodium bicarbonate, 1 mM EGTA, and 0.1% (w/v) BSA (pH 7.2)]. Reconstitution was then achieved by shaking ~10^8 gametocytes in 0.5 ml of CLB, supplemented with 5 μM coelenterazine for 30 min at 19°C. Loaded gametocytes were washed twice in CLB and were then suspended in 10 ml of RPMI 1640, 5% FBS, and 4 mM sodium bicarbonate (pH 7.2). For luminescence measurements, 10 μl of the gametocyte suspension were injected into 20 μl of SA or complemented with 150 μM XA or buffered at pH 7.8 (all at 4°C) in a 384-well assay plate of a FDSS μCELL (Hamamatsu Photonics) for a period of 5 min. The luminescence value of each time point was normalized to the initial luminescence value at 0 s ($L_{t=n}/L_{t=0}$).

Fluorescence lifetime imaging microscopy

P. berghei gametocytes and *P. falciparum* schizonts were purified as described above, and for each condition, 1 to 3 million parasites were resuspended in 500 μl of SA and incubated with 1 μM Flipper-TR for 15 min at 37°C. The parasites were washed twice with SA and resuspended in 500 μl of SA containing 16.2 μM Hoechst 33342 dye at pH 7.2. To test different conditions, 100 μM XA, 100 μM KA, or 5 μM BIPPO was added or the SA pH was increased to 7.8. The parasites were then centrifuged for 3 min at 600*g* at room temperature, and the pellet was resuspended in 5 to 10 μl of the individual SA medium, mounted on coverslips, and sealed.

Fluorescence lifetime imaging microscopy (FLIM) imaging was performed using a Leica TCS SP8 microscope fitted with a HC PL Apo 100×/1.40 numerical aperture oil CS2 objective and piloted with LAS X FLIM software (Leica Microsystems CMS GmbH). Samples were illuminated using a pulsed white laser at 488 nm for Flipper-TR and a ultraviolet laser line at 405 nm for Hoechst. Emission was collected with a hybrid detector for single-molecule detection (Leica HyD SMD) at 520 to 715 nm and 415 to 455 nm, respectively. Images were analyzed using the Leica LAS X FLIM software to fit acquired data from the regions of interest to a dual exponential model.

Protein immunoprecipitation and identification

Sample preparation

Co-immunoprecipitations (co-IPs) of PbGCα-3xHA and PbUGO-3xHA were performed with purified and nonactivated gametocytes. Samples were fixed for 10 min with 1% formaldehyde. IPs of *PfUGO-HA*:cKO were performed with saponin-lysed and nonactivated stage V gametocytes from cultures treated with DMSO or rapamycin. Parasites were lysed in radioimmunoprecipitation assay buffer [50 mM tris-HCl (pH 8), 150 mM NaCl, 1% NP-40, 0.5% sodium deoxycholate, and 0.1% SDS], and the supernatant was subjected to affinity purification with anti-HA antibody (Sigma-Aldrich) conjugated to magnetics beads. Beads were resuspended in 100 μl of 6 M urea in 50 mM AB. Two microliters of 50 mM dithioerythritol was added and the reduction was carried out at 37°C for 1 hour. Alkylation was performed by adding 2 μl of 400 mM iodoacetamide for 1 hour at room temperature in the dark. Urea was reduced to 1 M by addition of 500 μl of AB, and overnight digestion was performed at 37°C with 5 μl of freshly prepared trypsin (0.2 μg/μl; Promega) in AB. Supernatants were collected and completely dried under speed vacuum. Samples were then desalted with a C18 microspin column (Harvard Apparatus) according to the manufacturer's instructions, completely dried under speed vacuum, and stored at −20°C.

Liquid chromatography electrospray ionization tandem mass spectrometry

Samples were diluted in 20 μl of loading buffer [5% acetonitrile (CH_3CN) and 0.1% formic acid (FA)] and 2 μl was injected onto the column. Liquid chromatography electrospray ionization tandem mass spectrometry was performed either on a Q-Exactive Plus Hybrid Quadrupole-Orbitrap mass spectrometer (Thermo Fisher Scientific) equipped with an Easy nLC 1000 liquid chromatography system (Thermo Fisher Scientific) or an Orbitrap Fusion Lumos Tribrid mass spectrometer (Thermo Fisher Scientific) equipped with an Easy nLC 1200 liquid chromatography system (Thermo Fisher Scientific). Peptides were trapped on an Acclaim PepMap 100, 3 μm of C18, and 75-μm by 20-mm Nano-Trap column (Thermo Fisher Scientific) and separated on a 75-μm by 250-mm Q-Exactive or 500-mm Orbitrap Fusion Lumos, 2 μm of C18, and 100 Å of Easy-Spray column (Thermo Fisher Scientific). The analytical separation used a gradient of H_2O/0.1% FA (solvent A) and CH_3CN/0.1% FA (solvent B). The gradient was run as follows: 95% A and 5% B for 0 to 5 min, then to 65% A and 35% B for 60 min, then to 10% A and 90% B for 10 min, and finally 10% A and 90% B for 15 min. The flow rate was 250 nl/min for a total run time of 90 min.

Data-dependent analysis (DDA) was performed on the Q-Exactive Plus with MS1 full scan at a resolution of 70,000 full width at half maximum (FWHM) followed by MS2 scans on up to 15 selected precursors. MS1 was performed with an automatic gain control (AGC) target of 3×10^6, a maximum injection time of 100 ms, and a scan range from 400 to 2000 mass/charge ratio (m/z). MS2 was performed at a resolution of 17,500 FWHM with an AGC target at 1×10^5 and a maximum injection time of 50 ms. Isolation window was set at 1.6 m/z, and 27% normalized collision energy was used for higher-energy collisional dissociation (HCD). DDA was performed on the Orbitrap Fusion Lumos with MS1 full scan at a resolution of 120,000 FWHM followed by as many subsequent MS2 scans on selected precursors as possible within a 3-s maximum cycle time. MS1 was performed in the Orbitrap with an AGC target of 4×10^5, a maximum injection time of 50 ms, and a scan range from 400 to 2000 m/z. MS2 was performed in the ion trap with a rapid scan rate, an AGC target of 1×10^4, and a maximum injection time of 35 ms. The isolation window was set at 1.2 m/z, and 30% normalized collision energy was used for HCD.

Database searches

Peak lists (MGF file format) were generated from raw data using the MS Convert conversion tool from ProteoWizard. The peak list files were searched against the PlasmoDB_*P.berghei* ANKA database (PlasmoDB.org; release 38, 5076 entries) combined with an in-house database of common contaminants using Mascot (Matrix Science, London, UK; version 2.5.1). Trypsin was selected as the enzyme, with one potential missed cleavage. Precursor ion tolerance was set to 10 parts per million and fragment ion tolerance to 0.02 Da for Q-Exactive Plus data and to 0.6 for Lumos data. The variable amino acid modifications were oxidized methionine and deamination (Asn and Gln) as well as phosphorylated serine, threonine, and tyrosine. The fixed amino acid modification was carbamidomethyl cysteine. The Mascot search was validated using Scaffold 4.8.4 (Proteome Software) with 1% of protein false discovery rate (FDR) and at least two unique peptides per protein with a 0.1% peptide FDR.

Label-free comparison of peptide and phosphopeptides in GCα or UGO immunoprecipitates

Label-free comparison of peptide and phosphopeptides in GCα or UGO immunoprecipitates during the first minute of gametogony was determined using Proteome Discoverer 2.2 (Thermo Fisher Scientific). Peptide-spectrum matches were validated using the Percolator validator node with a target FDR of 0.01 and a Delta Cn of 0.5. For label-free quantification, features and chromatographic peaks were detected using the "Minora Feature Detector" node with the default parameters. Peptide-spectrum match (PSM) and peptides were filtered with an FDR of 1% and then grouped to proteins again with an FDR of 1% and using only peptides with high confidence level. Both unique and razor peptides were used for quantitation, and protein abundances are calculated by summing sample abundances of the connected peptide group. The abundances were normalized on the "Total Peptide Amount" and then "The pairwise Ratio Based" option was selected for protein ratio calculation, and associated P values were calculated with an analysis of variance (ANOVA) test based on background.

Reagents and antibodies

Rapamycin (LC Laboratories) was prepared in DMSO aliquots stored at −20°C (stock solution 20 μM) and used at 20 nM. The antifolate drug WR99210 was from Jacobus Pharmaceuticals (NJ, USA). Calcium ionophore A23187 (#C7522) and zaprinast (#Z0878), each

prepared in DMSO, were both from Sigma-Aldrich and used at 3 and 500 μM, respectively. BIPPO from Tonkin's laboratory (The University of Melbourne, Victoria, Australia) was used at 5 μM. XA from Sigma-Aldrich (#D120804) was prepared in 0.1 NaOH in water and used at 100 μM. PC (Avanti, catalog no. 850457) was solubilized at 5 mM in water:ethanol:methanol (1:1:2). Fluo-4 AM cell permeant was from Thermo Fisher Scientific. Flipper-TR was from Spirochrome.com, stock solution at 1 mM (catalog no. 020_21.02). SYBR Green I nucleic acid gel stain was from Thermo Fisher Scientific (catalog no. S7563). Oleic acid (Sigma-Aldrich, O1383) and palmitic acid (Sigma-Aldrich, P5585) were solved in 100% ethanol (stocks 30 mM). Aliquots were stored at −20°C and used at 30 μM. $NaHCO_3$ was from Sigma-Aldrich (31437-500G). BSA came from Sigma-Aldrich (A7906-100G). GlucNac came from (Sigma-Aldrich, A3286-100G/lot SLBX1976). Albumax medium was from GIBCO/Invitrogen (#11021-037). Hypoxanthine was from Sigma-Aldrich (#H9377), Hepes came from Sigma-Aldrich (# H4034), RPMI (+L-glutamine/−$NaHCO_3$) was from Thermo Fisher Scientific (#51800043), and neomycin powder was from Sigma-Aldrich (N6386-100G).

Dilutions and sources for antibodies for immunoblot or immunofluorescence analysis are as follows: anti-AMA1 (1:1000; rabbit; homemade), mouse anti-MSP1.19 mAb (1:1000; gift from M. Blackman, Francis Crick Institute, London, UK), and secondary antibodies goat anti-rabbit 594 (1:1000; Thermo Fisher Scientific, reference A11012) and goat anti-mouse 488 (1:1000; Thermo Fisher Scientific, reference A11001). Mouse anti-PfS25 (1:2000; Bei Resources, MRA-28), rabbit anti-g377 (1:1000; gift from P. Alano, National Institute of Health, Italy) (*67*), anti-mouse Alexa Fluor 594 (1:250; secondary; Invitrogen, A11032), and anti-rabbit 568 (1:250; Invitrogen, A11011).

Supplementary Materials

This PDF file includes:
Figs. S1 to S6
Legends for tables S1 to S4
Legend for data S1

Other Supplementary Material for this manuscript includes the following:
Tables S1 to S4
Data S1

View/request a protocol for this paper from *Bio-protocol*.

REFERENCES AND NOTES

1. C. R. Collins, F. Hackett, M. Strath, M. Penzo, C. Withers-Martinez, D. A. Baker, M. J. Blackman, Malaria parasite cGMP-dependent protein kinase regulates blood stage merozoite secretory organelle discharge and egress. *PLOS Pathog.* **9**, e1003344 (2013).
2. R. E. Sinden, The cell biology of sexual development in *Plasmodium*. *Parasitology* **86**, 7–28 (1983).
3. O. Billker, V. Lindo, M. Panico, A. E. Etienne, T. Paxton, A. Dell, M. Rogers, R. E. Sinden, H. R. Morris, Identification of xanthurenic acid as the putative inducer of malaria development in the mosquito. *Nature* **392**, 289–292 (1998).
4. D. S. Yamamoto, M. Sumitani, M. Hatakeyama, H. Matsuoka, Malaria infectivity of xanthurenic acid-deficient anopheline mosquitoes produced by TALEN-mediated targeted mutagenesis. *Transgenic Res.* **27**, 51–60 (2018).
5. M. Arai, O. Billker, H. R. Morris, M. Panico, M. Delcroix, D. Dixon, S. V. Ley, R. E. Sinden, Both mosquito-derived xanthurenic acid and a host blood-derived factor regulate gametogenesis of *Plasmodium* in the midgut of the mosquito. *Mol. Biochem. Parasitol.* **116**, 17–24 (2001).
6. V. L. A. Lima, F. Dias, R. D. Nunes, L. O. Pereira, T. S. R. Santos, L. B. Chiarini, T. D. Ramos, B. J. Silva-Mendes, J. Perales, R. H. Valente, P. L. Oliveira, The antioxidant role of xanthurenic acid in the *Aedes aegypti* midgut during digestion of a blood meal. *PLOS ONE* **7**, e38349 (2012).
7. O. Billker, A. J. Miller, R. E. Sinden, Determination of mosquito bloodmeal pH in situ by ion-selective microelectrode measurement: Implications for the regulation of malarial gametogenesis. *Parasitology* **120**, 547–551 (2000).
8. L. M. Smith, F. C. Motta, G. Chopra, J. K. Moch, R. R. Nerem, B. Cummins, K. E. Roche, C. M. Kelliher, A. R. Leman, J. Harer, T. Gedeon, N. C. Waters, S. B. Haase, An intrinsic oscillator drives the blood stage cycle of the malaria parasite *Plasmodium falciparum*. *Science* **368**, 754–759 (2020).
9. F. Rijo-Ferreira, V. A. Acosta-Rodriguez, J. H. Abel, I. Kornblum, I. Bento, G. Kilaru, E. B. Klerman, M. M. Mota, J. S. Takahashi, The malaria parasite has an intrinsic clock. *Science* **368**, 746–753 (2020).
10. A. S. Paul, A. Miliu, J. A. Paulo, J. M. Goldberg, A. M. Bonilla, L. Berry, M. Seveno, C. Braun-Breton, A. L. Kosber, B. Elsworth, J. S. N. Arriola, M. Lebrun, S. P. Gygi, M. H. Lamarque, M. T. Duraisingh, Co-option of *Plasmodium falciparum* PP1 for egress from host erythrocytes. *Nat. Commun.* **11**, 3532 (2020).
11. T. Mascher, J. D. Helmann, G. Unden, Stimulus perception in bacterial signal-transducing histidine kinases. *Microbiol. Mol. Biol. Rev.* **70**, 910–938 (2006).
12. N. Wettschureck, S. Offermanns, Mammalian G proteins and their cell type specific functions. *Physiol. Rev.* **85**, 1159–1204 (2005).
13. M. A. Lemmon, J. Schlessinger, Cell signaling by receptor tyrosine kinases. *Cell* **141**, 1117–1134 (2010).
14. U. Hohmann, K. Lau, M. Hothorn, The structural basis of ligand perception and signal activation by receptor kinases. *Annu. Rev. Plant Biol.* **68**, 109–137 (2017).
15. S. Köhler, C. F. Delwiche, P. W. Denny, L. G. Tilney, P. Webster, R. J. Wilson, J. D. Palmer, D. S. Roos, A plastid of probable green algal origin in Apicomplexan parasites. *Science* **275**, 1485–1489 (1997).
16. S. L. Baldauf, The deep roots of eukaryotes. *Science* **300**, 1703–1706 (2003).
17. M. Brochet, M. O. Collins, T. K. Smith, E. Thompson, S. Sebastian, K. Volkmann, F. Schwach, L. Chappell, A. R. Gomes, M. Berriman, J. C. Rayner, D. A. Baker, J. Choudhary, O. Billker, Phosphoinositide metabolism links cGMP-dependent protein kinase G to essential Ca^{2+} signals at key decision points in the life cycle of malaria parasites. *PLoS Biol.* **12**, e1001806 (2014).
18. D. K. Muhia, C. A. Swales, W. Deng, J. M. Kelly, D. A. Baker, The gametocyte-activating factor xanthurenic acid stimulates an increase in membrane-associated guanylyl cyclase activity in the human malaria parasite *Plasmodium falciparum*. *Mol. Microbiol.* **42**, 553–560 (2001).
19. L. R. Potter, Guanylyl cyclase structure, function and regulation. *Cell. Signal.* **23**, 1921–1926 (2011).
20. D. A. Baker, J. M. Kelly, Structure, function and evolution of microbial adenylyl and guanylyl cyclases. *Mol. Microbiol.* **52**, 1229–1242 (2004).
21. K. M. Brown, L. D. Sibley, Essential cGMP signaling in *Toxoplasma* is initiated by a hybrid P-type ATPase-guanylate cyclase. *Cell Host Microbe* **24**, 804–816.e6 (2018).
22. C. J. Taylor, L. McRobert, D. A. Baker, Disruption of a *Plasmodium falciparum* cyclic nucleotide phosphodiesterase gene causes aberrant gametogenesis. *Mol. Microbiol.* **69**, 110–118 (2008).
23. R. W. Moon, C. J. Taylor, C. Bex, R. Schepers, D. Goulding, C. J. Janse, A. P. Waters, D. A. Baker, O. Billker, A cyclic GMP signalling module that regulates gliding motility in a malaria parasite. *PLOS Pathog.* **5**, e1000599 (2009).
24. H. Gao, Z. Yang, X. Wang, P. Qian, R. Hong, X. Chen, X. Z. Su, H. Cui, J. Yuan, ISP1-anchored polarization of GCβ/CDC50A complex initiates malaria ookinete gliding motility. *Curr. Biol.* **28**, 2763–2776.e6 (2018).
25. S. D. Nofal, A. Patel, M. J. Blackman, C. Flueck, D. A. Baker, *Plasmodium falciparum* guanylyl cyclase-alpha and the activity of its appended P4-ATPase domain are essential for cGMP synthesis and blood-stage egress. *MBio* **12**, e02694-20 (2021).
26. Y. Jiang, J. Wei, H. Cui, C. Liu, Y. Zhi, Z. Z. Jiang, Z. Li, S. Li, Z. Yang, X. Wang, P. Qian, C. Zhang, C. Zhong, X. Z. Su, J. Yuan, An intracellular membrane protein GEP1 regulates xanthurenic acid induced gametogenesis of malaria parasites. *Nat. Commun.* **11**, 1764 (2020).
27. D. A. Baker, L. B. Stewart, J. M. Large, P. W. Bowyer, K. H. Ansell, M. B. Jiménez-Díaz, M. el Bakkouri, K. Birchall, K. J. Dechering, N. S. Bouloc, P. J. Coombs, D. Whalley, D. J. Harding, E. Smiljanic-Hurley, M. C. Wheldon, E. M. Walker, J. T. Dessens, M. J. Lafuente, L. M. Sanz, F. J. Gamo, S. B. Ferrer, R. Hui, T. Bousema, I. Angulo-Barturén, A. T. Merritt, S. L. Croft, W. E. Gutteridge, C. A. Kettleborough, S. A. Osborne, A potent series targeting the malarial cGMP-dependent protein kinase clears infection and blocks transmission. *Nat. Commun.* **8**, 430 (2017).
28. C. Flueck, L. G. Drought, A. Jones, A. Patel, A. J. Perrin, E. M. Walker, S. D. Nofal, A. P. Snijders, M. J. Blackman, D. A. Baker, Phosphodiesterase beta is the master regulator of cAMP signalling during malaria parasite invasion. *PLoS Biol.* **17**, e3000154 (2019).

29. D. A. Baker, L. G. Drought, C. Flueck, S. D. Nofal, A. Patel, M. Penzo, E. M. Walker, Cyclic nucleotide signalling in malaria parasites. *Open Biol.* **7**, 170213 (2017).
30. L. McRobert, C. J. Taylor, W. Deng, Q. L. Fivelman, R. M. Cummings, S. D. Polley, O. Billker, D. A. Baker, Gametogenesis in malaria parasites is mediated by the cGMP-dependent protein kinase. *PLOS Biol.* **6**, e139 (2008).
31. O. Billker, M. K. Shaw, G. Margos, R. E. Sinden, The roles of temperature, pH and mosquito factors as triggers of male and female gametogenesis of Plasmodium berghei in vitro. *Parasitology* **115**, 1–7 (1997).
32. G. E. Garcia, R. A. Wirtz, J. R. Barr, A. Woolfitt, R. Rosenberg, Xanthurenic acid induces gametogenesis in *Plasmodium*, the malaria parasite. *J. Biol. Chem.* **273**, 12003–12005 (1998).
33. M. Brochet, A. C. Balestra, L. Brusini, cGMP homeostasis in malaria parasites—The key to perceiving and integrating environmental changes during transmission to the mosquito. *Mol. Microbiol.* **115**, 829–838 (2021).
34. M. Brochet, O. Billker, Calcium signalling in malaria parasites. *Mol. Microbiol.* **100**, 397–408 (2016).
35. O. Billker, S. Dechamps, R. Tewari, G. Wenig, B. Franke-Fayard, V. Brinkmann, Calcium and a calcium-dependent protein kinase regulate gamete formation and mosquito transmission in a malaria parasite. *Cell* **117**, 503–514 (2004).
36. L. Wentzinger, S. Bopp, H. Tenor, J. Klar, R. Brun, H. P. Beck, T. Seebeck, Cyclic nucleotide-specific phosphodiesterases of *Plasmodium falciparum*: PfPDEalpha, a non-essential cGMP-specific PDE that is an integral membrane protein. *Int. J. Parasitol.* **38**, 1625–1637 (2008).
37. N. Philip, A. P. Waters, Conditional degradation of *Plasmodium* calcineurin reveals functions in parasite colonization of both host and vector. *Cell Host Microbe* **18**, 122–131 (2015).
38. K. Yuasa, F. Mi-Ichi, T. Kobayashi, M. Yamanouchi, J. Kotera, K. Kita, K. Omori, PfPDE1, a novel cGMP-specific phosphodiesterase from the human malaria parasite *Plasmodium falciparum*. *Biochem. J.* **392**, 221–229 (2005).
39. A. Patel, S. D. Nofal, M. J. Blackman, D. A. Baker, CDC50 orthologues in *Plasmodium falciparum* have distinct roles in merozoite egress and trophozoite maturation. *MBio* **13**, e0163522 (2022).
40. K. Segawa, S. Kurata, S. Nagata, The CDC50A extracellular domain is required for forming a functional complex with and chaperoning phospholipid flippases to the plasma membrane. *J. Biol. Chem.* **293**, 2172–2182 (2018).
41. H. Bisio, M. Lungi, M. Brochet, D. Soldati, Phosphatidic acid governs natural egress in *Toxoplasma gondii* via a guanylate cyclase receptor platform. *Nat. Microbiol.* **4**, 420–428 (2019).
42. W. Li, J. Grech, J. F. Stortz, M. Gow, J. Periz, M. Meissner, E. Jimenez-Ruiz, A splitCas9 phenotypic screen in *Toxoplasma gondii* identifies proteins involved in host cell egress and invasion. *Nat. Microbiol.* **7**, 882–895 (2022).
43. S. Ye, M. Lungi, D. Soldati-Favre, A signaling factor linked to *Toxoplasma gondii* guanylate cyclase complex controls invasion and egress during acute and chronic infection. *MBio* **13**, e0196522 (2022).
44. M. Zhang, C. Wang, T. D. Otto, J. Oberstaller, X. Liao, S. R. Adapa, K. Udenze, I. F. Bronner, D. Casandra, M. Mayho, J. Brown, S. Li, J. Swanson, J. C. Rayner, R. H. Y. Jiang, J. H. Adams, Uncovering the essential genes of the human malaria parasite Plasmodium falciparum by saturation mutagenesis. *Science* **360**, eaap7847 (2018).
45. A. J. Perrin, C. R. Collins, M. R. G. Russell, L. M. Collinson, D. A. Baker, M. J. Blackman, The actinomyosin motor drives malaria parasite red blood cell invasion but not egress. *mBio* **9**, e00905-18 (2018).
46. T. F. de Koning-Ward, A. Olivieri, L. Bertuccini, A. Hood, F. Silvestrini, K. Charvalias, P. Berzosa Díaz, G. Camarda, T. McElwain, T. Papenfuss, J. Healer, L. Baldassarri, B. S. Crabb, P. Alano, L. C. Ranford-Cartwright, The role of osmiophilic bodies and Pfg377 expression in female gametocyte emergence and mosquito infectivity in the human malaria parasite *Plasmodium falciparum*. *Mol. Microbiol.* **67**, 278–290 (2008).
47. M. J. Delves, A. Ruecker, U. Straschil, J. Lelièvre, S. Marques, M. J. López-Barragán, E. Herreros, R. E. Sinden, Male and female *Plasmodium falciparum* mature gametocytes show different responses to antimalarial drugs. *Antimicrob. Agents Chemother.* **57**, 3268–3274 (2013).
48. E. Bushell, A. R. Gomes, T. Sanderson, B. Anar, G. Girling, C. Herd, T. Metcalf, K. Modrzynska, F. Schwach, R. E. Martin, M. W. Mather, G. I. McFadden, L. Parts, G. G. Rutledge, A. B. Vaidya, K. Wengelnik, J. C. Rayner, O. Billker, Functional profiling of a *Plasmodium* genome reveals an abundance of essential genes. *Cell* **170**, 260–272.e8 (2017).
49. B. Mons, C. J. Janse, E. G. Boorsma, H. J. Van der Kaay, Synchronized erythrocytic schizogony and gametocytogenesis of *Plasmodium berghei in vivo* and *in vitro*. *Parasitology* **91**, 423–430 (1985).
50. A. L. Dearsly, R. E. Sinden, I. A. Self, Sexual development in malarial parasites: Gametocyte production, fertility and infectivity to the mosquito vector. *Parasitology* **100**, 359–368 (1990).
51. A. Colom, E. Derivery, S. Soleimanpour, C. Tomba, M. D. Molin, N. Sakai, M. González-Gaitán, S. Matile, A. Roux, A fluorescent membrane tension probe. *Nat. Chem.* **10**, 1118–1125 (2018).
52. A. C. Balestra, K. Koussis, N. Klages, S. A. Howell, H. R. Flynn, M. Bantscheff, C. Pasquarello, A. J. Perrin, L. Brusini, P. Arboit, O. Sanz, L. P.-B. Castaño, C. Withers-Martinez, A. Hainard, S. Ghidelli-Disse, A. P. Snijders, D. A. Baker, M. J. Blackman, M. Brochet, Ca^{2+} signals critical for egress and gametogenesis in malaria parasites depend on a multipass membrane protein that interacts with PKG. *Sci. Adv.* **7**, eabe5396 (2021).
53. J. S. Shah, P. S. Soon, D. J. Marsh, Comparison of methodologies to detect low levels of hemolysis in serum for accurate assessment of serum microRNAs. *PLOS ONE* **11**, e0153200 (2016).
54. S. Gulati, E. H. Ekland, K. V. Ruggles, R. B. Chan, B. Jayabalasingham, B. Zhou, P.-Y. Mantel, M. C. S. Lee, N. Spottiswoode, O. Coburn-Flynn, D. Hjelmqvist, T. S. Worgall, M. Marti, G. di Paolo, D. A. Fidock, Profiling the essential nature of lipid metabolism in asexual blood and gametocyte stages of *Plasmodium falciparum*. *Cell Host Microbe* **18**, 371–381 (2015).
55. S. Bennink, M. J. Kiesow, G. Pradel, The development of malaria parasites in the mosquito midgut. *Cell. Microbiol.* **18**, 905–918 (2016).
56. H. Fang, N. Klages, B. Baechler, E. Hillner, L. Yu, M. Pardo, J. Choudhary, M. Brochet, Multiple short windows of calcium-dependent protein kinase 4 activity coordinate distinct cell cycle events during *Plasmodium* gametogenesis. *eLife* **6**, e26524 (2017).
57. H. Bisio, A. Krishnan, J. B. Marq, D. Soldati-Favre, *Toxoplasma gondii* phosphatidylserine flippase complex ATP2B-CDC50.4 critically participates in microneme exocytosis. *PLOS Pathog.* **18**, e1010438 (2022).
58. M. S. Roiko, N. Svezhova, V. B. Carruthers, Acidification activates *Toxoplasma gondii* motility and egress by enhancing protein secretion and cytolytic activity. *PLOS Pathog.* **10**, e1004488 (2014).
59. C. Zhu, X. Liang, X. Chen, M. Liang, J. Zheng, B. Wan, S. Luo, Characterizing the specific recognition of xanthurenic acid by GEP1 and GEP1-GCα interactions in cGMP signaling pathway in gametogenesis of malaria parasites. *Int. J. Mol. Sci.* **24**, 2561 (2023).
60. C. Pfander, B. Anar, M. Brochet, J. C. Rayner, O. Billker, Recombination-mediated genetic engineering of *Plasmodium berghei* DNA. *Methods Mol. Biol.* **923**, 127–138 (2013).
61. C. Pfander, B. Anar, F. Schwach, T. D. Otto, M. Brochet, K. Volkmann, M. A. Quail, A. Pain, B. Rosen, W. Skarnes, J. C. Rayner, O. Billker, A scalable pipeline for highly effective genetic modification of a malaria parasite. *Nat. Methods* **8**, 1078–1082 (2011).
62. E. Knuepfer, M. Napiorkowska, C. van Ooij, A. A. Holder, Generating conditional gene knockouts in *Plasmodium*—A toolkit to produce stable DiCre recombinase-expressing parasite lines using CRISPR/Cas9. *Sci. Rep.* **7**, 3881–3881 (2017).
63. L. Vincke, M. Lips, Un nouveau *Plasmodium* d'un rongeur sauvage du Congo. *Plasmodium berghei* n.sp. *Ann. Soc. Belg. Med. Trap* **28**, 97–104 (1948).
64. C. R. Collins, S. das, E. H. Wong, N. Andenmatten, R. Stallmach, F. Hackett, J.-P. Herman, S. Müller, M. Meissner, M. J. Blackman, Robust inducible Cre recombinase activity in the human malaria parasite *Plasmodium falciparum* enables efficient gene deletion within a single asexual erythrocytic growth cycle. *Mol. Microbiol.* **88**, 687–701 (2013).
65. Q. L. Fivelman, L. McRobert, S. Sharp, C. J. Taylor, M. Saeed, C. A. Swales, C. J. Sutherland, D. A. Baker, Improved synchronous production of *Plasmodium falciparum* gametocytes *in vitro*. *Mol. Biochem. Parasitology* **154**, 119–123 (2007).
66. L. J. Leba, L. Musset, S. Pelleau, Y. Estevez, C. Birer, S. Briolant, B. Witkowski, D. Ménard, M. J. Delves, E. Legrand, C. Duplais, J. Popovici, Use of Plasmodium falciparum culture-adapted field isolates for in vitro exflagellation-blocking assay. *Malar. J.* **14**, 234 (2015).
67. P. Alano, D. Read, M. Bruce, M. Aikawa, T. Kaido, T. Tegoshi, S. Bhatti, D. K. Smith, C. Luo, S. Hansra, R. Carter, J. F. Elliott, COS cell expression cloning of Pfg377, a *Plasmodium falciparum* gametocyte antigen associated with osmiophilic bodies. *Mol. Biochem. Parasitol.* **74**, 143–156 (1995).
68. C. Miguel-Blanco, J. Lelièvre, M. J. Delves, A. I. Bardera, J. L. Presa, M. J. López-Barragán, A. Ruecker, S. Marques, R. E. Sinden, E. Herreros, Imaging-based high-throughput screening assay to identify new molecules with transmission-blocking potential against *Plasmodium falciparum* female gamete formation. *Antimicrob. Agents Chemother.* **59**, 3298–3305 (2015).
69. H. Fang, A. R. Gomes, N. Klages, P. Pino, B. Maco, E. M. Walker, Z. A. Zenonos, F. Angrisano, J. Baum, C. Doerig, D. A. Baker, O. Billker, M. Brochet, Epistasis studies reveal redundancy among calcium-dependent protein kinases in motility and invasion of malaria parasites. *Nat. Commun.* **9**, 4248 (2018).

Acknowledgments: We thank the excellent support of the core facilities at the Faculty of Medicine of the University of Geneva: J.-P. Aubry-Lachainaye and C. Gameiro (flow cytometry); N. Walter, C. Heckenmeyer, D. Schvartz, C. Pasquarello, and A. Hainard (proteomics); Y. Cambet (calcium imaging); and F. Prodon, N. Liaudet, and O. Brun (bioimaging). We thank the service of the flow cytometry facility at the University of Lausanne (F. Sala de Oyanguren and K. Blackney). We also thank O. Vadas for discussions and A. Roux (University of Geneva) for advices on the Flipper-TR probe. **Funding:** This work was supported by the Swiss National Science Foundation

(grant BSSGI0_155852 to M.B., grant CRSII5_198545 to D.S. and M.B., and grant 310030_184785 to T.S.V.) and by the Fondation privée des Hôpitaux Universitaires de Genève (CONFIRM grant RC05-10) to M.B. and D.S. B.M. was funded by the European Research Council under the European Union's Horizon 2020 Research and Innovation program under grant agreement no. 695596. **Author contributions:** Conceptualization: M.B. and D.S. Formal analysis: R.M.K., E.G., A.C.B., C.S., and M.B. Funding acquisition: M.B., D.S., N.B., and T.S.V. Investigation: R.M.K., E.G., A.C.B., C.S., L.B., B.M., and M.W. Method development: N.B. Supervision: M.B., D.S., N.B., and T.S.V. Writing—original draft: M.B. Writing—review and editing: all authors. **Competing interests:** The authors declare that they have no competing interests. **Data and materials availability:** All data needed to evaluate the conclusions in the paper are present in the paper and/or the Supplementary Materials. The mass spectrometry proteomics data have been deposited to the ProteomeXchange Consortium via the PRIDE partner repository (http://proteomecentral.proteomexchange.org) with the dataset identifier PXD035569.

Submitted 7 October 2022
Accepted 11 May 2023
Published 16 June 2023
10.1126/sciadv.adf2161

ScienceAdvances

A *Plasmodium* membrane receptor platform integrates cues for egress and invasion in blood forms and activation of transmission stages

Ronja Marie Kuehnel, Emma Ganga, Aurlia C. Balestra, Catherine Suarez, Matthias Wyss, Natacha Klages, Lorenzo Brusini, Bohumil Maco, Nicolas Brancucci, Till S. Voss, Dominique Soldati, and Mathieu Brochet

Sci. Adv., **9** (24), eadf2161.
DOI: 10.1126/sciadv.adf2161

Science Advances (ISSN) is published by the American Association for the Advancement of Science. 1200 New York Avenue NW, Washington, DC 20005. The title *Science Advances* is a registered trademark of AAAS.